Developmental Biology 448 (2019) 183–198

Contents lists available at ScienceDirect

Developmental Biology

journal homepage: www.elsevier.com/locate/developmentalbiology

Papillae revisited and the nature of the adhesive secreting collocytes

Fan Zeng[a,1], Julia Wunderer[a,1], Willi Salvenmoser[a], Michael W. Hess[b], Peter Ladurner[a], Ute Rothbächer[a,*]

[a] Evolutionary Developmental Biology, Institute of Zoology, University Innsbruck, Technikerstr. 25, A-6020 Innsbruck, Austria
[b] Division of Histology and Embryology, Innsbruck Medical University, Muellerstrasse 59, A-6020 Innsbruck, Austria

ARTICLE INFO

Keywords:
Ascidian
Sensory adhesive organ
Papillae
Palps
PNS
Collocytes

ABSTRACT

Ascidian papillae (palps) constitute a transient sensory adhesive organ that assures larval settlement and the onset of metamorphosis to the filterfeeding adult. Despite the importance of papillae for the ascidian development, their cellular composition is only roughly described. For *Ciona intestinalis/robusta,* a clear definition of cell numbers and discriminative molecular markers for the different cell types is missing. While some attention was given to neural cell types and their connectivity little is known about the adhesive producing collocytes. We converge serial-section electron microscopy and confocal imaging with various marker combinations to document the 3D organization of the *Ciona* papillae. We show the papillar development with 4 axial columnar cells (ACCs), 4 lateral primary sensory neurons (PSNs) and 12 central collocytes (CCs). We propose molecular markers for each cell type including novel ones for collocytes. The subcellular characteristics are suggestive of their role in papillar function: the ACCs featuring apical protrusions and microvilli, also contain neuroactive and endocytic vesicles indicative of a chemosensory role. They are clearly distinct from the ciliated glutamatergic PSNs. CCs encircle the ACCs and contain microvilli, small endocytic vesicles and notably a large numbers of adhesive granules that, according to element analysis and histochemistry, contain glycoproteins. Interestingly, we detect two different types of collocyte granules, one of them containing fibrous material and larger quantities of polysaccharides. Consistently, carbohydrate specific lectins label the papillar apex, the granules within CCs and the adhesive plaques upon larval attachment. We further propose CCs to derive from an evolutionary ancient neurosecretory cell type. Our findings contribute to understanding the development of the anterior ('new head') region of the *Ciona* larva and notably the adhesive secreting cells which has implications for developmental biology, cell differentiation and evolution, but also bioadhesion.

1. Introduction

Ascidians are marine, mostly sessile organisms, and as part of the Tunicates, the vertebrate sister group within chordates (Delsuc et al., 2006). They are remarkable through a swimming tadpole larva that teaches us about ancestral chordate innovations, such as sensory structures greatly expanded in the vertebrate head including the cranial placodes (Manni et al., 2004; Mazet and Shimeld, 2005; Schlosser et al., 2014; Patthey et al., 2014) or the neural crest (Abitua et al., 2012). Ascidians are also one of the major biofoulers populating natural and artificial surfaces with important consequences for marine shipping and aquaculture (Aldred and Clare, 2014). Knowledge on the mechano-sensory and adhesive properties for ascidian larval settlement and the building up during development in cellular and molecular terms is thus relevant to both, the understanding of the emergence of the vertebrate 'new head' but also to developing biomimetic medicinal glues or green anti-adhesives.

Ascidians, while particularly close to vertebrates in phylogenetic terms, are very well amenable to developmental, cellular and molecular experimentation. Notably, for the model organism *Ciona intestinalis/robusta,* a well expanded toolbox for functional genomics analyses is in place (Dehal et al., 2002; Imai et al., 2006; Roure et al., 2007; Tassy et al., 2010; Stolfi et al., 2014; Gilchrist et al., 2015; Kari et al., 2016; Database portals at http://tunicate-portal.org/resources-2/resources).

Ascidians, while forming gregarious populations of solitary or colonial adults always possess a free-swimming larva (with few exceptions) as a dispersal stage in their life cycle. The free-swimming period is rather short and mainly serves to inspect the substratum, then settle and rebuild an adult (Cloney, 1977). Ascidian larval adhesion is thus essential to initiate metamorphosis and its failure leads to fatal

* Corresponding author.
E-mail address: ute.rothbaecher@uibk.ac.at (U. Rothbächer).
[1] Equal contribution.

https://doi.org/10.1016/j.ydbio.2018.11.012
Received 30 May 2018; Received in revised form 17 November 2018; Accepted 20 November 2018
Available online 22 November 2018
0012-1606/ © 2018 Published by Elsevier Inc.

defects (Kimura et al., 2003; Nakayama-Ishimura et al., 2009; Sasakura et al., 2012; reviewed in Karaiskou et al., 2015). The three adhesive organs (palps or papillae) extend the anterior larval head in a normally triangular arrangement and are surrounded by the tunic composed of two layers. The outer layer is very prominent in the tail to form the larval fin and is discarded during metamorphosis while the inner layer is more prominent in the larval trunc and forms the outer surface of juveniles and adults after metamorphosis (Cloney, 1977). Despite a variable organization in different species (Cloney, 1977), each papilla is generally composed of at least three different cell types: axial columnar cells, primary sensory neurons and adhesive secreting cells (collocytes), all ending their elongated cellular extensions in a hyaline cap at the distal apex. The papillar extensions are thought to sense and likely taste the substrate (Pennati et al., 2007) for settlement initiated with adhesive material being secreted from the papillar apex (reviewed in Pennati and Rothbacher, 2015).

The comparison of the adhesive organs between species also points to controversies and still open questions, with the characterization of *Ciona* adhesive organs only at their beginning (Dolcemascolo et al., 2009; Wagner et al., 2014). While previous ultrastructural analyses have implicated further cell types in other species, notably two different types of collocytes and additional accessory cells (Cloney, 1977), confusion still reigns about the number of cell types in papillar extensions in *Ciona* (Wagner et al., 2014). Notably, the number of neural cell types and their neurotransmitters and the exact function, notably in adhesion remains unclear. At least eight neurons (Imai and Meinertzhagen, 2007) and various neurotransmitters (Horie et al., 2008) are being discussed (Takamura et al., 2010).

Several markers label the *Ciona* papillae including ßγ-crystallin (Shimeld et al., 2005), synaptotagmin (Sakurai et al., 2004) or neurotransmitter components including the vesicular glutamate transporter VgluT (Horie et al., 2008). These markers may distinguish between the different cell types but their co-expression was not thoroughly examined. Very little is known about the adhesive secreting cells (the collocytes) and notably the molecular nature of the adhesive(s) produced, to what extent curing occurs, through which component(s) (Lane, 1973) and, whether/how initial larval attachment is molecularly linked to permanent settlement during metamorphosis. The role of the hyaline cap remains controversial with its circumpapillary apical space thought to be filled with secretory material and discussed to play a role in initial attachment (Cloney, 1977) but thought non-adhesive in other species (Caicci et al., 2010).

Towards a better understanding of the *Ciona* adhesive papillae and to define novel markers for the different adhesive cells we have started with two strategies, one is, revisiting the ultrastructure with state-of-the-art techniques, and the second is, inspired from Bioadhesion research in other marine organisms, with Lectin stainings. Lectin staining is frequently used in adhesion research to identify and localize specific sugar residues on glycoproteins present in adhesive organs and adhesive plaques of several marine invertebrates (Lengerer et al., 2014). Using specific lectin stainings on sea star tube feet, Hennebert and colleagues have identified eight glycoproteins that are also present in sea star adhesive plaques, the material left on the substratum after detachment (Hennebert et al., 2011).

Thus, using such carbohydrate markers, we have analysed the *Ciona* papillae and have combined the analysis of cellular and cytoskeletal markers from confocal imaging with insights from serial-section electron microscopy to document in more detail the 3D organization, in both cellular and molecular terms, that will be instrumental for further functional studies. Notably, we could newly associate each of the different cell types with discriminating markers, we could determine the exact cell numbers and have discovered two different types of granules in the adhesive cells. The developmental suite demonstrates a very early specification of cell types in the papillar primordium with adhesive granule production starting amongst the first events.

2. Material and methods

2.1. Animals and larvae

Ciona intestinalis or *Ciona robusta* (Pennati and Rothbacher, 2015) adults were purchased from Roscoff Marine Station, France, and kept in an aquarium with circulating and oxygenated artificial seawater with HEPES (ASWH) at 16 °C until usage. Fertilization and embryo culturing were performed as described (Kari et al., 2016).

2.2. Plasmid construction and electroporation

The two reporter plasmids *synaptotagmin*-GFP (*pSyt* > GFP) (Katsuyama et al., 2002) and *Ciona vesicular glutamate Transporter*-GFP (*pVgluT* > GFP) drive expression in papillar neurons of *Ciona intestinalis* (Imai and Meinertzhagen, 2007; Horie et al., 2008) and were kindly provided by A. Pasini.

The synaptotagmin-mCherry construct (*pSyt* > mCherry) was generated by replacing GFP with mCherry in the *pSyt* > GFP plasmid using *BamH*I and *Not*I restriction enzymes. The coding sequence of mCherry fluorescent protein (mCherry) was PCR amplified from pFOGL > mCherry (Roure et al., 2007) using the primers: mCherry-forward (5'-CCGG ATCCACCGGTCGCCACCATGGTGAGCAAGGGCGAGG-3') and mCherry-reverse (5'-CCGCGGCCGCTTTACTTGTACAGCTCGTCCATGC-3').

Plasmids for *pSyt* > GFP, *pSyt* > mCherry and/or *pVgluT* > GFP were used at a final concentration of 50 µg/50 µl in electroporation, as described previously (Kari et al., 2016).

2.3. Immunofluorescence staining of larvae

Specimen were fixed with 4% paraformaldehyde (PFA) in 1× phosphate buffered saline (PBS) for 30 min, washed three times with PBS, then gradually dehydrated to 100% menthol and stored at – 20 °C. After stepwise rehydration to 100% PBS, samples were permeabilized with 0.1% (w/v) Triton X-100 in PBS (PBS-T). Non-specific antibody binding was blocked with 3% (w/v) bovine serum albumin (BSA) in PBS-T for 1 h at room temperature and incubated in primary antibody in BSA-PBS-T. Primary antibodies were: rabbit-anti-Ci-ßγ-Crystallin (kindly provided by SM Shimeld) (Shimeld et al., 2005), mouse anti-Ci-synaptotagmin polyclonal (kindly provided by Takehiro Kusakabe) (Katsuyama et al., 2002; Imai and Meinertzhagen, 2007), rabbit-anti-GFP (Life technologies, 1512093) or mouse-anti-GFP (Roche, 1181446001), mouse-anti-Acetylated-Tubulin (Sigma, 070114755), all diluted 1:500; mouse-anti-α-Tubulin (Sigma, T5168), diluted 1:1000, at 4 °C overnight. After several washing-steps with PBS-T at room temperature, they were incubated in secondary antibody, either goat anti-rabbit Alexafluor 488 (Life technologies, A31627) or Alexafluor 568 (Life technologies, A11011), or goat anti-mouse Alexafluor 488 (Life technologies, A11029) or Alexafluor 555 (Life technologies, A21422) diluted 1:500 in BSA-PBS-T. Samples were washed with PBS several times, mounted with Vectashield (Vector laboratories, CA94010), and imaged using the Leica SP5 II confocal scanning microscopy. Stacks of optical sections from 0.3 µm to 0.8 µm were acquired sequentially and z-projected. Images were analysed with ImageJ (Version 1.52 h).

2.4. Lectin fluorescence histochemistry

Larvae or adhesive plaques were fixed in 4% PFA in PBS for 30 min and rinsed three times in Tris-buffered saline (pH 8.0) supplemented with 5 mM $CaCl_2$ and 0.1% Triton X-100 (TBS-T). Unspecific background staining was blocked by pre-incubation in TBS-T containing 3% *(w/v)* bovine serum albumin (BSA-TBS-T) for 1 h at room temperature. Biotinylated Peanut Agglutinine (PNA; B-1075, Vector Laboratory) was diluted in BSA-TBS-T to a final concentration of 25 µg/ml and applied to the specimen overnight at 4 °C. After six

washes of 10 min each in TBS-T, larvae were incubated for 1 h in Dylight488-conjugated-streptavidin (SA-5488, Vector Laboratories) or Texas-Red-conjugated-streptavidin (SA-5006, Vector Laboratory) diluted 1:300 in BSA-TBS-T at room temperature. After several washing steps in TBS-T, larvae were mounted in Vectashield and analysed using a Leica SP5 II confocal scanning microscope. Stacks were acquired sequentially and z-projected. Images were analysed with ImageJ (Version 1.52 h).

Control reactions for PNA labelling were performed by pre-incubating the lectin with its inhibitory monosaccharide D-galactose (0.2 M) for 2 h at 4 °C.

2.5. Collection of adhesive plaques

Adhesive plaques were collected as follows: freshly hatched wild type larvae (18 hpf) were put on a petri dish covered with 1% agarose and filled with ASWH (artificial seawater buffered with HEPES, pH 8) containing 0,5% BSA. A square glass cover slip was placed at the bottom of a petri dish. Adhesive competent larvae (~ 24 hpf) were allowed to settle on the glass slide and forced to detach using the water flow of a Pasteur pipette. The remaining adhesive plaques on the glass slide were PNA stained according to the Lectin histochemistry protocol described in the previous section.

2.6. Crystal violet staining of adhesive plaques

Adhesive plaques collected on a square glass or plastic slide (see previous section) were rinsed with ASWH, and incubated with crystal violet staining buffer (0.05% crystal violet in Hydra medium, see Rodrigues et al., 2016) for 30 min at room temperature. Slides were rinsed with Millipore water, air-dried, and analysed using a Leica DM5000 microscope.

2.7. Electron microscopy

Ciona intestinalis larvae collected at 18, 20, 24 and 26 hpf were chemically fixed simultaneously with glutaraldehyde and osmium tetroxide according to Eisenman and Alfert (1982), dehydrated and embedded in EMbed 812 resin. Additional samples were chemically fixed with 2.5% glutaraldehyde in 0.1 M cacodylate buffer containing 10% sucrose for 1 h at 4 °C, rinsed with cacodylate buffer and post fixed with 1% osmium tetroxide in 0.05 M cacodylate buffer for 1 h at 4 °C. After washing in cacodylate buffer, samples were dehydrated with an acetone series and embedded in resin. Longitudinal and cross sections of papillae were cut with a diamond knife (Diatome, Switzerland) and an Ultracut UCT (Leica, Austria), mounted on grids, stained with lead citrate and examined with a Libra 120 energy filter transmission electron microscope (TEM, from Zeiss, Germany). Images were made with a TRS 2 × 2k high speed camera (Tröndle, Germany) and an iTEM software (Olympus, Japan). Brand and cat numbers: EMbed 812812 (EMS, 14900/13710/19000/11400), glutaraldehyde (Agar Scientific, R102), lead citrate (Merck 1.07398) osmium tetroxide (Electron Microscopy Sciences (EMS), 19110), perjodic acid (Carl Roth 3257), sodium cacodylate (Sigma, 49945), uranyl acetate (EMS 541–09-3), silverproteinate (Etablissements ROQUES Nr.: 13243), sucrose (Sigma S7903), thiocarbohydracide (FLUKA 88535).

2.8. High-pressure freezing and freeze-substitution (referred to as cryofixation in the remaining text)

Ciona intestinalis larvae collected at 26 hpf were high-pressure frozen with a BALTEC-HPM-010 (Balzers, Lichtenstein), freeze-substituted in acetone supplemented with 1% Osmium tetroxide and 0.2% uranyl acetate by using an AFS2 device (Leica Microsystems, Austria) and embedded into EMBed 812 epoxy resin (Salvenmoser et al., 2010). Thin sections were optionally stained with uranyl acetate and lead citrate and examined with a CM 120 TEM (Philips/Fisher Thermoscientific, Netherlands). Images were taken with a MORADA CCD camera (oSIS, Olympus, Japan). Polysaccharides with vicinal hydoxyl groups were detected with the periodic acid-thiocarbohydrazide-silver proteinate reaction (PA-TCH-SP, the EM-correlate of the histological periodic acid-Schiff-reaction: (Thiéry, 1967) as previously described (Hess and Hesse, 1994). Omission of the periodic acid oxidation step served as negative control (TCH-SP; see Hess and Hesse, 1994 and references therein).

2.9. Element analysis with EELS and ESI

Electron energy loss spectroscopy (EELS) and electron spectroscopic imaging (ESI) are well established methods to demonstrate elements in biological tissue (Gammoudi et al., 2016). Nitrogen (N) was measured spectroscopically and identified by its energy loss at 397 eV at the N-K edge. ESI was performed with a three window method of the iTEM software. High contrast images at 250 eV electron loss were made, inverted and mix mapped with the maximum element distribution in false color images.

2.10. Measurement of cilia length

The length of cilia were measured with iTEM software (Olympus, Japan), the data were processed with bivariate statistic program, one-way ANOVA, of Statistical Package for the Social Science (SPSS) statistics software (IBM, Corporation).

3. Results

3.1. Peanut agglutinin as a novel marker for adhesive secreting cells in Ciona

In search of cell type specific markers for the different cell types within the *Ciona* papillae, and notably the adhesive secreting ‚collocytes', we screened the carbohydrate fraction often specific to adhesive organs in marine organisms (Hennebert et al., 2011; Lengerer et al., 2016; Zeng et al., manuscript in preparation). We found Biotinylated Peanut Agglutinin (PNA) to specifically bind to both, the tips of *Ciona* papillae (Fig. 1A, D) and to punctate, proximal locations within the papillar body (Fig. 1A). The punctate staining was not visible in older, partially adhering larvae where papillar tips had opened and PNA positive material seemed to leak out at the apical tip of the hyline cap (Fig. 1D). PNA did not fully overlap with the known palp marker ßγ−crystallin (Fig. 1B, C, E, F; Suppl. Video 1) and thus constitutes a separate cell population. This staining pattern suggests that PNA stains the adhesive material produced within the adhesive vesicles of collocytes and accumulated in the hyline cap to be secreted with the larval attachment.

Supplementary material related to this article can be found online at doi:10.1016/j.ydbio.2018.11.012.

To independently show that PNA recognizes the adhesive material, we stained the adhesive plaques left behind on the substrate of adhering larvae that are gently washed away by a pipetting seawater flow. Indeed adhesive plaques strongly bound PNA (Fig. 1G) suggesting that PNA associates to both, the adhesive producing cells and the secreted adhesive itself.

Crystal violet stains proteinaceous material (Feoktistova et al., 2016) with *Ciona* larval adhesive plaques (Fig. 1H) being visible as a thin layer around a central adhesive core (likely strongly stained by PNA in Fig. 1G) suggesting that the adhesive material contains glycoproteins.

Consistently, following a higher resolution analysis of papillar tips in electron microscopic cross-sections (Fig. 1I–L), the collocyte granules appeared enriched in nitrogen, characteristic of proteins, respectively, as determined by element analysis with electron spectroscopic

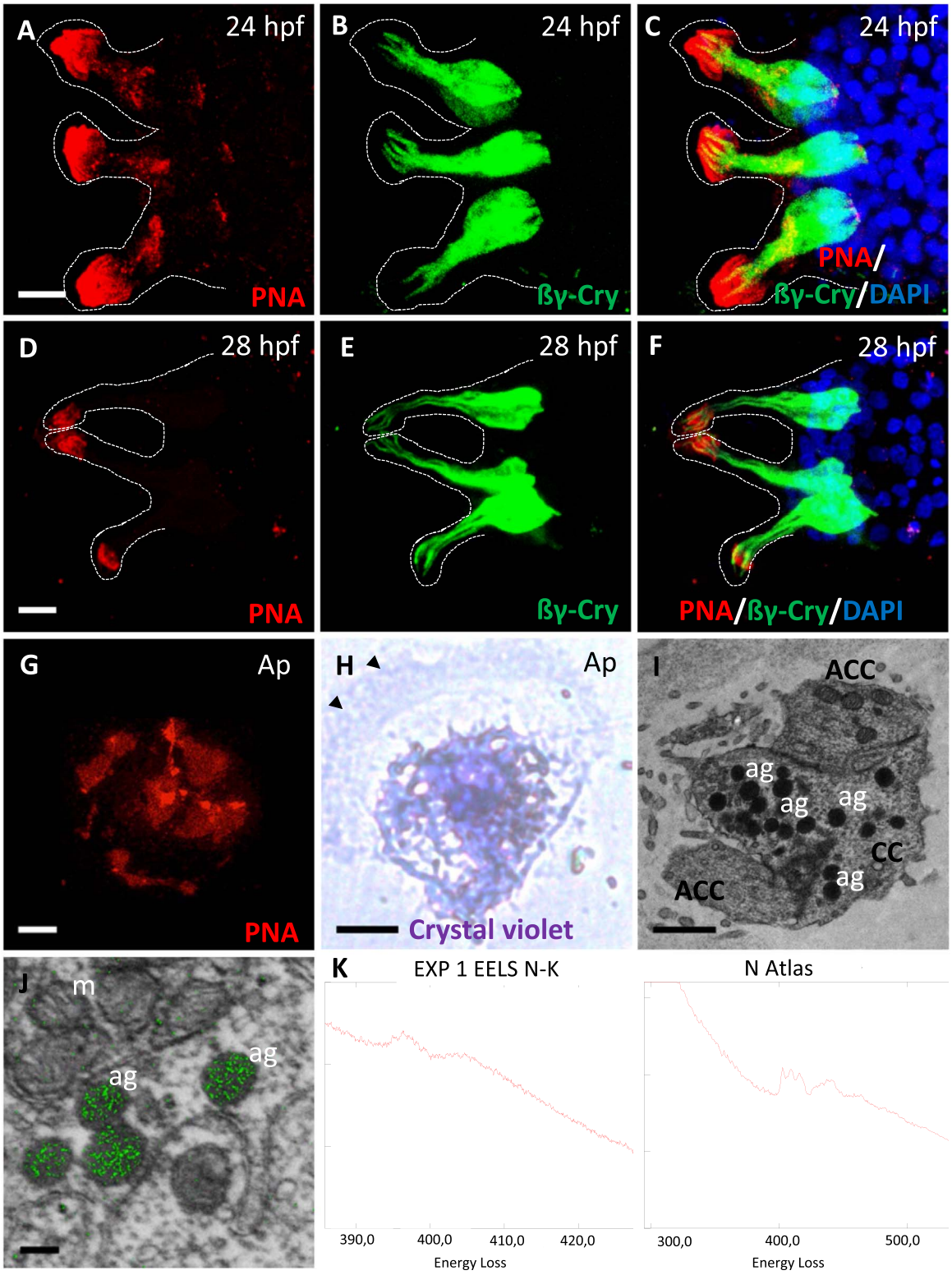

Fig. 1. PNA is a novel marker for adhesive secreting collocytes in *C. intestinalis*. (A–E) Confocal projections of triple labelling of adhesive papillae with Lectin PNA (red) in cell bodies of adhesive producing collocytes (CCs) and in the hyaline cap, with ßγ-Crystallin antibody staining (green) in axial columnar cells (ACCs), and with nuclear DAPI staining (blue) in 24 hpf (A–C) and 28 hpf (D–F) larvae. (G–H) Adhesive plaque (Ap) secretion left on the substrate after forced larval detachment. (G) PNA labelling of secreted material. (H) Crystal violet staining, black arrowheads indicate the edge of the film-like plaque. (I–L) Ultrastructural analysis of CC adhesive granules in Transmission electron microscopy (TEM). (I) cross section of one adhesive papilla with a central CC and two flanking ACCs. Note the electron dense adhesive granules (ag) in the CC. (J) Electron spectroscopy imaging (ESI) of CC granules (ag) for nitrogen enrichment (green) strongly indicates their proteinaceous nature (compare unlabelled mitochondria, *m*, nearby). (K), (L) EELS graph of Nitrogen (N) measurement in electron energy loss spectroscopy (EELS) on the adhesive granules in (J) as compared to the N standard in the atlas (EELS graph of boronitride evaporated film as control). Dotted lines indicate the outline of papillae. *ACC* axial columnar cells, *CC* collocytes, *ag* adhesive granules, *m* mitochondria. Scale bars: (A–H) 10 µm, (I) 1 µm.

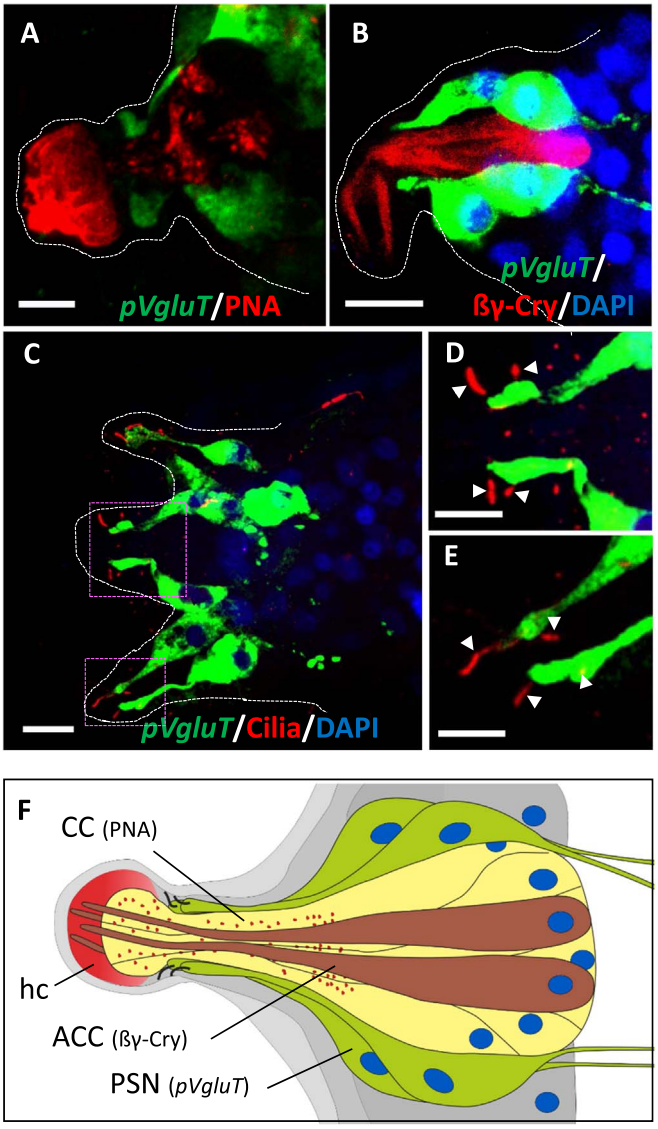

Fig. 2. Three molecular markers discriminate the three papillar cell populations. (A–E) Confocal projections of adhesive papillae in *pVglutT* > GFP transgenic larvae marking primary sensory neurons (PSNs) with GFP (green). (A) Double labelling in a single papilla of PSNs (green) and CCs with PNA (red). (B) Triple labelling in a single papilla of PSNs (green) and ACCs with a ßγ-Crystallin antibody (red) and nuclei with DAPI (blue). (C) Triple labelling in all three adhesive papillae of PSNs (green) and cilia with an acetylated tubulin antibody (red), and nuclei with DAPI (blue). Dotted lines indicate the outline of papillae. Rectangles in (C) indicate zoomed-in areas in (D, E) white arrowheads indicate cilia. (F) Scheme of the papillar cell types and their discriminating markers. Four ACCs in a mid central position (brown, ßγ-Crystallin positive) are surrounded by CCs (yellow) that contain abundant granules with adhesive (red, PNA positive) that accumulates in the apical hyaline cap (hc, red, PNA positive). The ACCs reach their apical protrusions far into the hyaline cap. ACCs and CCs are flanked by four PSNs (green, *pVglut* > GFP positive) with cilia protruding from their apical thickenings (black lines). Epithelial cells (dark gray) surround the base of the organ and most nuclei are located in the basal part of the cell, while the entire organ is covered with two layers of tunic. Scale bar: (A–C) 10 µm (D, E) 5 µm.

imaging (ESI, Fig. 1J) and electron energy loss spectroscopy (EELS, Fig. 1K and L).

We conclude that PNA marks both, the collocytes in the *Ciona* papillae and their glycoproteinaceous adhesive material.

3.2. Discriminative molecular markers for the three papillar cell populations

Since the PNA bound to collocytes but did not colocalise with ßγ-crystallin labeled cells (Fig. 1C and F) we compared the PNA staining with another known palp marker, the transporter for vesicular glutamate (Horie et al., 2008). PNA staining did not overlap with the VgluT marked cell population (*pVglutT* > GFP) either (Fig. 2A). Remarkably, VgluT and ßγ-crystallin positive cells were exclusive, too (Fig. 2B). VgluT marked cells had a lower, lateral position with a spindled shape and proximal axons, suggesting that they constitute the primary sensory neurons (PSNs). These cells are known to be ciliated, which we could confirm with an antibody recognizing acetylated tubulin (Fig. 2C–E). Indeed, each of the three papillae contained two pairs of single ciliated primary sensory neurons where the cells of each pair were tightly connected but slightly shifted in their relative position and had distally flattened endings with a central cilium (Fig. 2D, E). By contrast, ßγ-crystallin positive cells had a characteristic central position within the papillae and digitiform protrusions extending far into the hyaline cap (Fig. 2B and Fig. 1B, C, E, F), constituting features typical of axial columnar cells (ACCs). Overall, we thus found bona fide distinct markers for three different cell populations within the *Ciona* papillae that are schematically represented in Fig. 2F.

3.3. Ultrastructural characteristics suggestive of a role in papillar function

To determine more accurately the relative position, subcellular features and the exact number of the different cell types, we revisited the *Ciona* papillar sensory adhesive organ by Transmission Electron Microscopy (TEM) in longitudinal, sagittal sections (Fig. 3, Fig. S1) and, notably, in serial cross sections (Fig. 4, Figs. S2–S6).

In TEM images of late stages of adhesion competent *Ciona* larvae (26 hpf) we detected collocytes (CCs, Fig. 3A,B) with frequently densely packed adhesive granules (Fig. 4A, B; Fig. 1I). Collocytes generally formed a rounded apical platform with thin microvilli protruding into the hyline cap (hc) (Fig. 3). Some late stage larvae had an open hyaline cap with broken surrounding tunic layers (Fig. S1C), supposedly after having attached. CCs were intermingled with the axial columnar cells (ACCs) that extended their cytoplasm far into the apical hyaline cap, forming fingerlike protrusions of around 5 µm in length and 2 µm in diameter (Fig. S1). Ciliated primary sensory neurons (PSNs), in contrast, ended more proximally and in a lateral position within the apical papillar shaft (Fig. 2). Apically, all external and lateral cells were connected to each other by densely stained, belt like tight junctions/zonulae occludens (Fig. 3).

The relative positions of the three cell types became even more evident in serial TEM cross sections of the papillae (Figs. 4, 5 and Figs. S2–S6). Rostral to caudal cross sections of a 26 hpf larva were TEM imaged from their distal most (rostral, anterior) portion that included the hyaline cap up to slightly beyond the proximal insertion in the epidermal layer. The distal most cross sections (Fig. 4A, Figs. S2–S4) showed the ACCs prominently extending into the hyaline cap surrounded by hyaline cap material and the inner and outer tunic membranes. ACCs were interspersed by central CCs that featured the typical electron dense adhesive granules. Apical microvilli from the adjacent CCs extended into the hyaline cap. In slightly more proximal sections (Fig. 4B, Figs. S2–S4), ACCs were entirely surrounded by CCs sometimes leaving a narrow cell free space around the ACC extensions, possibly to allow for their bending within the hyaline cap. PSNs, appeared more proximally (Fig. 4B, Figs. S2–S3) and were consistently more lateral and in opposite position, featuring a cilium that extended in apico-lateral direction towards the inner tunic layer.

At a subcellular level, ACCs (Fig. 4C, D) featured a large number of microtubules, actin filaments, clathrin coated pits and endocytic vesicles, as well as a number of neuroactive vesicles: dense vesicles of 130 nm diameter (likely peptidergic), dense core vesicles of 180–280 nm (likely aminergic) and lucent vesicles of ≈ 104 nm (likely cholinergic). No cilia were seen but we detected a centriole at a proximal position (data not shown). CCs contained adhesive granules of

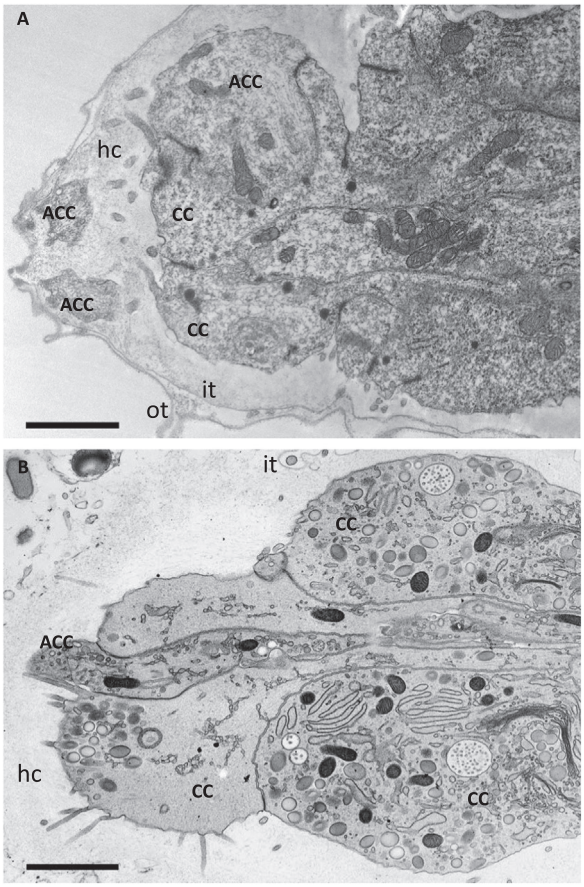

Fig. 3. The ultrastructure of the cell types of adhesive papillae. TEM images of an adhesive papilla in longitudinal sections, upon (A) chemical fixation (24 hpf larva) and (B) cryofixation (26 hpf larva). *ACC* axial columnar cells, *CC* collocytes, *it* inner tunic, *ot* outer tunic, *hc* hyaline cap. Scale bars: 2 µm.

approximately 300 nm in size (Fig. 4E, F) and showed endocytic activity through clathrin coated pits (Fig. 4E). CC likewise contained microtubules and actin filaments. Most surprisingly, however, we found apically localized basal bodies in the CCs but no cilia (Fig. 4F). The cilia present in PSNs were of the non-motile 9 + 2 type lacking dynein arms and were located –at least partly– within a cytoplasmic invagination, thus surrounded by a cytoplasm-free space in the apical most region (Fig. 4G, Fig. S3).

The three cell types therefore contain common cytoskeletal features but exclusive specialisations reflecting their likely functions. The presence of apical basal bodies in CCs could represent a specialization from common precursors with PSNs.

3.4. Collocytes contain two types of granules

A closer inspection of the collocyte granules in chemically fixed TEM sections showed some heterogeneity in the granule population pointing to possibly two different types. For a more reliable ultrastructure preservation we analysed cryofixed samples by subsequent TEM imaging. Indeed, two cleary distinguishable large types of large granules were contained in the collocytes (Fig. 5). The first granule type (dark arrowheads in Fig. 5A–F) was spherical to ellipsoid in shape, with quite homogenous contents (“smooth”) and measured ≈ 330 nm in length and ≈ 210 nm in width (Suppl. Table 1A). The second type of granules (white arrowheads in Fig. 5A–F) was less abundant, round in shape, with a more or less wrinkled limiting membrane – a quite uncommon, but still unexplained feature of natively cryofixed organelles; these granules had fibrous contents and were slightly smaller with an average size of 280 nm (Suppl. Table 1B).

In addition, to better characterize these two granule types we stained with periodic acid-thiocarbohydrazide-silver proteinate (PA-TCH-SP; Fig. 5C, D), that labels certain polysaccharides (Thiéry, 1967; Hess and Hesse, 1994). Indeed, the granules showed very differential staining patterns. The ellipsoid, “smooth” granules all showed a clearly PA-TCH-SP-positive dark rim, but the staining intensities of the granules’ core varied considerably (Fig. 5C). The second “wrinkled” granule type stained more or less uniformely strong and consistently displayed fibrous contents (Fig. 5D). In control samples, TCH-SP bound merely to the lipids of the membranes (Fig. 5 E, F).

Overall, EM of natively cryofixed samples clearly revealed two types of granules intermingled within the collocytes. On the basis of data available it is likely that the abundant, ellipsoid granules contain glycoproteins (consistent with Fig. 1I–L), while the fibrous granules carry higher amounts in polysaccharides. The exact composition of the two collocyte granules remains to be determined in future studies.

3.5. Twenty papillar cells with more than half being collocytes

By serial TEM cross sectioning we could also determine the exact cell number within the three *Ciona* papillae (Fig. 6). We followed the cells in consecutive sections down to a cutting depth of 10 µm that corresponds to the level of the most distal (PSNs) cell nuclei (see also Fig. 1 and Fig. S2 and Fig. S3), thus completely covering the protruding part of all three papillae. We identified individual cells according to their relative position, shape and size, in each papilla, then color-coded and numbered the cells according to their distal appearance, counting separately for each cell type. The papillar cell number was of exactly 20 (Fig. 6), and equal in all three papillae (Fig. S5 and Fig. S6): 4 ACCs (visualized in brown), seemingly linked by membranes, were surrounded by 12 CCs (yellow) and flanked by lower 2 pairs of PSNs, both ciliated (pink). Generally, the 4 ACCs seemed of similar length, extending apically into the hyaline cap, while more central CCs, notably those surrounding the ACCs, were distally extending relative to the lateral CCs. A lateral shortening was also seen in the PSNs. This cellular constellation produced an apically rounded papillar body.

Overall, sagittal and transversal TEM sections revealed a very consistent picture of the three larval papillae with central 4 ACCs, intermingled by 12 CCs and flanked by 2 twins of more proximally ending PSNs.

3.6. Synaptotagmin reporter expression reveals a common history of PSNs and collocytes

The presence of related subcellular structures like basal bodies and cilia or the presence of various vesicles types and granules in all three palp cell types, raised the question of whether the cells may have specialized from a common ancestral neuroepithelial cell type, such as a ciliated neurosecretory cell (also discussed in Pennati and Rothbacher, 2015). Notably synaptotagmin may hint to such ancestry as it marks vesicle producing cells and is thought to be expressed in the ascidian palp neurons (Katsuyama et al., 2002; Imai and Meinertzhagen, 2007), while it remains unclear whether other cell types could stain as well. We thus reanalysed both, the synaptotagmin regulatory region driving GFP as well as the antibody recognizing the *Ciona* synaptotagmin protein in conjunction with the here defined cell type specific markers for CCs (PNA), ACCs (ßγ-crystallin) or PSNs (VgluT and acetylated tubulin for cilia).

Interestingly, in *synaptotagmin* > GFP (*pSyt* > GFP) transgenic larvae we observed mosaics that labeled cells in a central palp position while others were positioned more laterally and had a spindled shape typical of PSNs indicating that more than one cell type could be labeled (Fig. 7). Clearly, in co-stainings, *pSyt* > GFP overlapped with the centrally located PNA labeled CCs (Fig. 7A–C, Suppl. Video 2). To more directly show that synaptotagmin is expressed in PSNs, we generated a construct where synaptotagmin drove mCherry (*pSyt* >

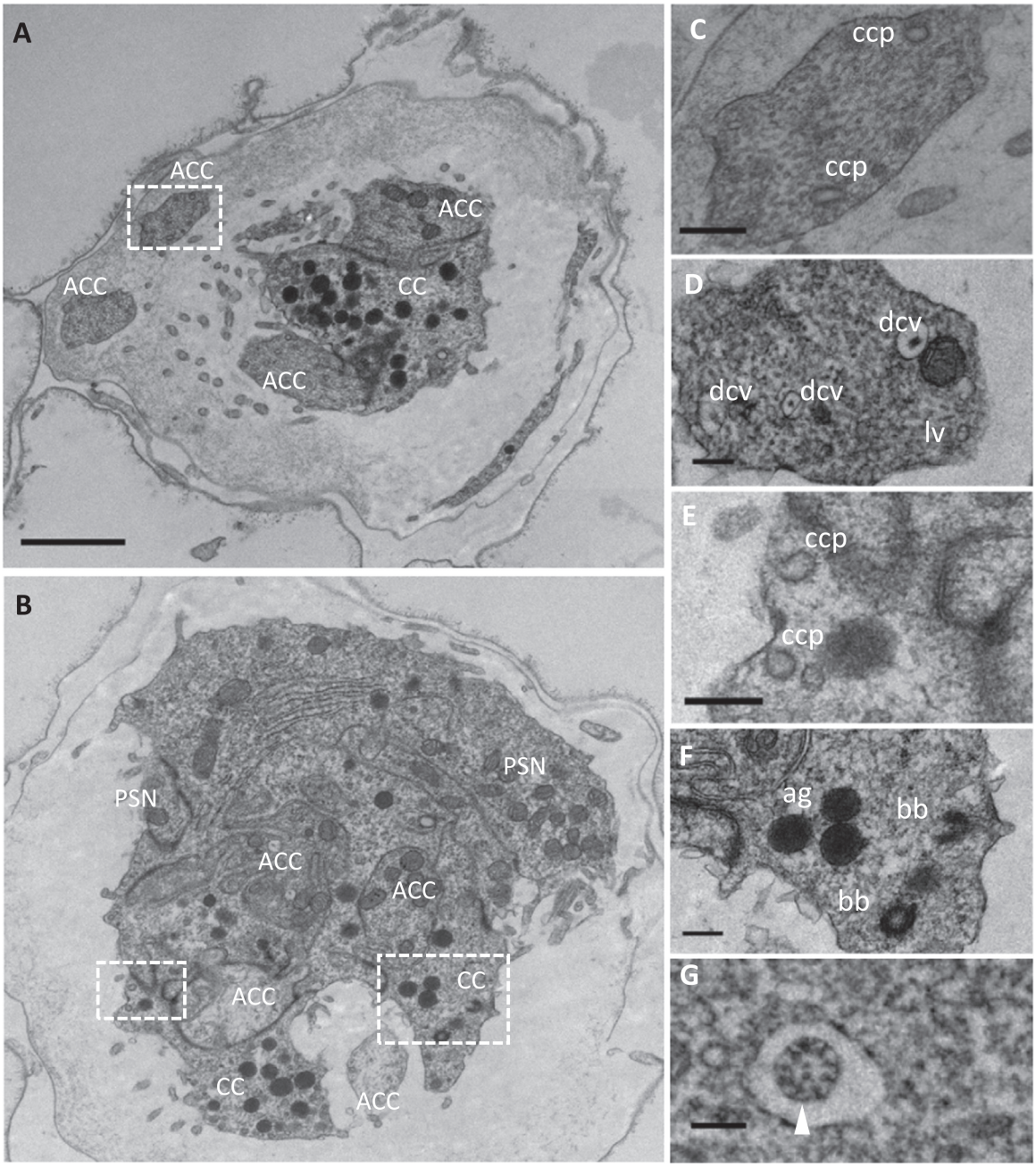

Fig. 4. Subcellular features are suggestive of the papillar cellular functions. TEM images of adhesive papillae in cross sections, upon chemical fixation (26 hpf larva). (A) Cross section 2 µm from rostral to caudal of papilla Nr. 1. (B) cross section 2 µm from rostral to caudal of papilla Nr. 2. (C, D) details in ACC digitiform protrusions with clathrin coated pits (ccp) (C) and two additional vesicle types (D). (E, F) Details of CCs containing electron-dense adhesive granules, but also ccp (F) and two basal bodies (bb) (E). (G) detail of a PSN featuring a sensory cilium with the typical 9 + 2 structure without dynein arms. White rectangles in (A) and (B) indicate the area of enlargement in (C, E, F). Overviews to (D) and (G) are shown in Fig. S2B and Fig. S3K, respectively. *ACC* axial columnar cells, *ag* adhesive granule, *bb* basal bodies, *CC* collocytes, *ccp* clathrin coated pits, *dcv* dense core vesicle, *lv* lucent vesicle, PSN primary sensory neuron, white arrowhead points to a sensory cilium. Scale bar: (A) 2 µm, (B) 1 µm, (C-G) 250 nm.

mCherry, Fig. 7E) and produced double transgenic larve with *pVgluT* > GFP (Fig. 6D) to mark the PSNs. Indeed, a co-localization could be seen for synaptotagmin and VgluT markers that included portions of proximal axons (Fig. 7F) confirming the synaptotagmin gene expression in the PSNs. In addition, we produced triple stained larvae with *pSyt* > GFP, PNA and the cilia marker to show that CCs and PSNs were simultaneously labeled by synaptotagmin (Fig. 7G–I, pink arrows point to the cilia). In contrast, when we stained *pSyt* > GFP larvae with the ACC marker ßγ-crystallin (Fig. 7J–L) we could not obtain a clear overlap (Suppl. Video 3). Indeed, the GFP and TexasRed marked cells seemed tightly intermingled while GFP positive cells that featured a flattened apex typical of the centrally located collocytes and were seemingly pierced by ßγ-crystallin positive ACC protrusions at their apical ends, a picture consistent with the TEM results above (Figs. 3–5). For an independent evaluation of synaptotagmin expression, we used an antibody directed against Ci-synaptotagmin (Sakurai et al., 2004) and co-stained with anti-ßγ-crystallin (Fig. 7M–O). Now, the papillae were strongly stained all over with apical tips and axons more intensely labeled than the rounded papillar bodies (Fig. 7M). Here, the ßγ-crystallin positive apical extensions were well labeled with the synaptotagmin antibody (Fig. 7O). The latter is consistent with the presence of smaller vesicles in the ACCs evidenced in TEM (Fig. 4C, D). The synaptotagmin antibody labelling may therefore reflect the actual vesicular activity in all the cells at this given stage. This contrasts with the synaptotagmin transgene expression, that rather reflects the history of the synaptotagmin gene expression in the cell lineages with the GFP

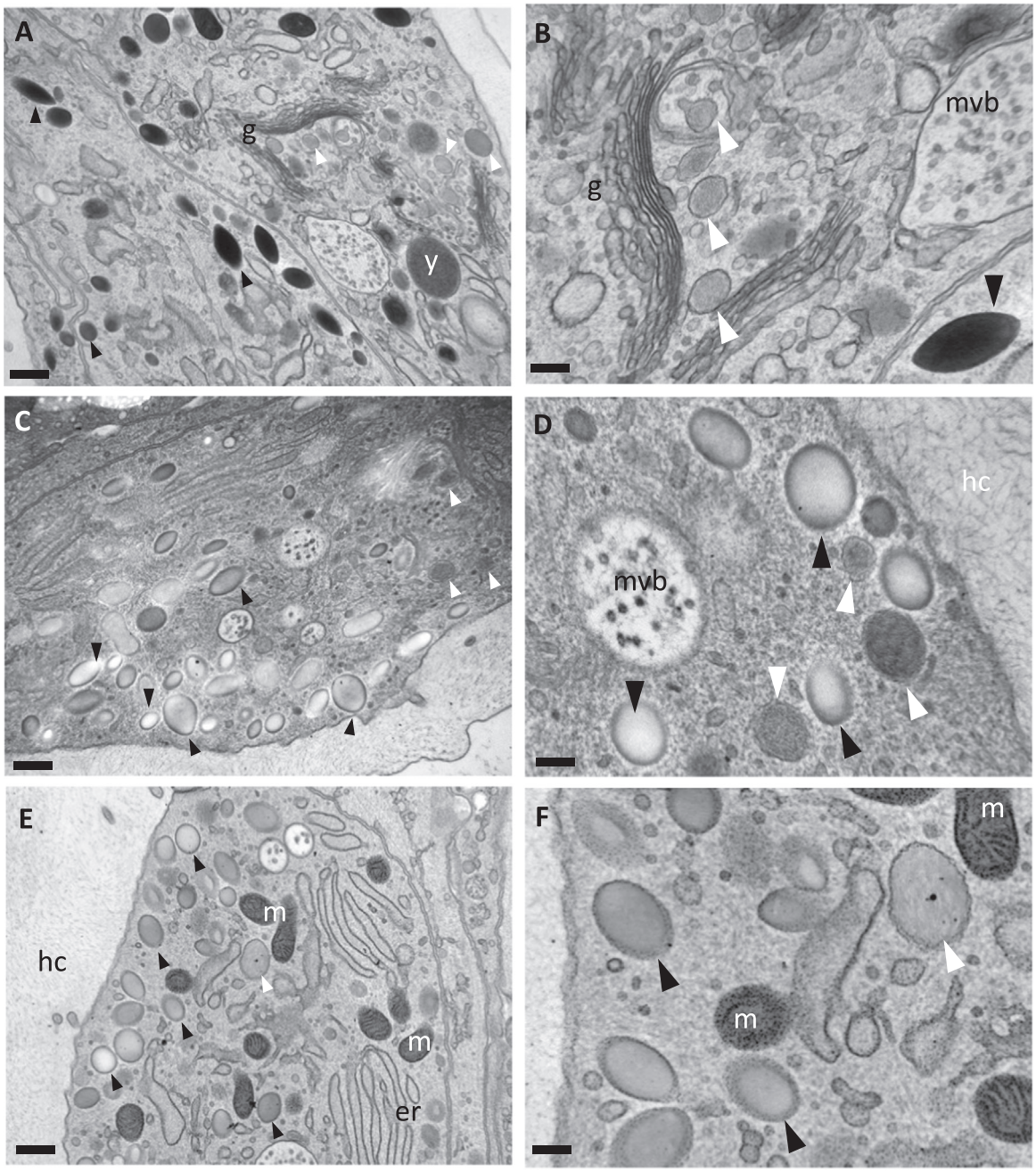

Fig. 5. Two types of large granules are contained in one adhesive cell type. TEM images of adhesive papillae, upon cryofixation (26 hpf larvae). (A), (B) Two types of adhesive granules can be distinguished: spherical to ellipsoid (sometimes even spindle-shaped), electron dense granules (black arrowheads) and spherical, moderately dense granules (white arrowheads) with fibrous contents, as seen after standard uranyl acetate and lead section staining. (C), (D) Periodic acid-thiocarbohydrazide-silverproteinate (PA-TCH-SP) staining of CC granules shows clear differences in staining intensity between the two granule types, as well as variable staining throughout the ellipsoid, "smooth" granule population. (E), (F) TCH-SP staining of lipids serving as control for PA-TCH-SP. *er* endoplasmic reticulum, *g* Golgi apparatus, *hc* hyaline cap, *m* mitochondrium, *mvb* multivesicular body, *y* yolk. Scale bar: (A), (C), (E) 500 nm, (B), (D), (F) 200 nm.

signal accumulating over time, and more strongly in the CC and PSN lineages. Taken together, the synaptotagmin transgene expression points to a closer relatedness of CCs and PSNs, which, again, is consistent with a common ontogeny and/or ancestry of these two cell types (Summarized in Suppl. Table 2).

Supplementary material related to this article can be found online at doi:10.1016/j.ydbio.2018.11.012.

3.7. Collocytes form first and are actively secreting from the earliest stages onwards

Freeswimming *Ciona* larvae undergo a developmental maturation of their papillae after hatching that successively increases their competence to attach and settle for subsequent metamorphosis (Davidson and Swalla, 2002; reviewed in Karaiskou et al., 2015). Initially small papillar protrusions at 18 hpf successively elongate towards mature adhesive papillae (Fig. S7) that by 28 hpf have expelled secretory material to crosslink to almost any type of substrate they encounter, including siblings.

To gain insight into the developmental suite and the timed emergence of the different cell types and their functions from the palp precursor field we analysed various stages of developing larvae, from 18 to 28 h post fertilization (hpf). We analysed the developing cells with both, the discriminating differentiation markers (PNA for CCs, ßγ-

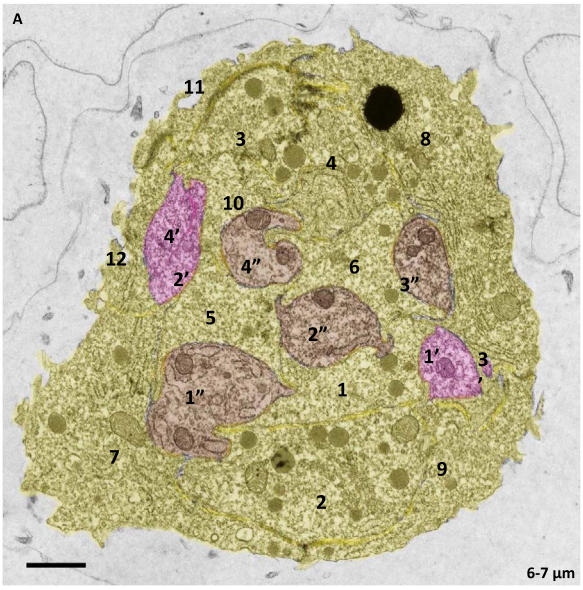

Fig. 6. Each adhesive papilla of *C. intestinalis* comprises 20 cells. TEM image, cross section of adhesive papilla Nr. 2 of a *C. intestinalis* larva (26 hpf), section at 6–7 µm from rostral to caudal. The 20 cells are false coloured and comprise four PSNs (1'–4', pink), four ACCs (1"–4", brown) and twelve CCs (1–12, yellow). Scale bar: 1 µm.

crystallin for ACCs and VgluT and acetylated tubulin for the cilia, both for PSNs) and combined them with cell structural markers of typical subcellular characteristics, such as α-tubulin for microtubules enriched in protruding ACCs (Fig. 8), phalloidin for actin bundles enriched in microvilli extending largely from the collocytes (Fig. 9) or, synaptotagmin for vesicular function (Fig. 10).

To observe the developmental emergence of ACCs we performed double stainings with antibodies recognizing βγ-crystallin and α-tubulin and counterstained the nuclei with DAPI (Fig. 8). Early 18 hpf stages (Fig. 8A) featured a flattened bud of papillar outgrowth with a moderate enrichment of microtubules at the apical site of elogating epithelial cells. βγ-crystallin became weakly visible slightly later, at 20 hpf (Fig. 8B, red) when the protruding papillar epithelium was more pyramidal in shape. Microtubules now extended basally into the epithelium forming an oval shaped papillar cone and were more clearly enriched at the apical side (Fig. 8B, green). At 22 hpf (Fig. 8C) the papillae have dramatically elongated and acquired a round bottom flask shape with elongated βγ-crystallin positive cells extending far into the rounded protrusion. A dense meshwork of longitudinal microtubule fibres surrounded the papillar cones and formed small extensions at distal and axons at the proximal part. During the following stages (Fig. 8D–F) the papillae continued the elongation of the papillar shaft and towards the outside with apical cellular protrusions extending far into the apical area of the hyaline cap. From these results we conclude that microtubules are dramatically associated to shaping the developing papillae (18–25 hpf), while during the later, adhesion competent stages they are concentrated around the four cellular extensions of ACCs in the hyaline cap and the papillar axons (supposedly of PSNs). ACCs start expressing their cell type specific differentiation marker at 20 hpf concommitant with early papillar outgrowth.

The emergence of PSNs was observed with the cilia marker acetylated tubulin and compared to the actin filament distribution enriched in the apical microvillar extensions by using phallodin (Fig. 9). Early papillar buds (Fig. 9A) showed only moderate actin enrichment and no cilia. This changed at 20 hpf (Fig. 9B) where multiple actin foci were well visible in papillar buds and 2 tiny cilia became visible more basally. At 22 hpf (Fig. 9C) both actin fibres and cilia had extended within the elongating papillae, a process that continued up to around 27 hpf (Fig. 9C–G). A magnified view of the ciliary region (Fig. 8H and I) of the 22 hpf larva shows the lateral positions of 2 cilia on the papillar shaft and extending from adjacent cells that are surrounded by actin filaments. When measuring the cilia length of sibling larvae at different stages of development (Fig. 9J) we could show their linear lengthening from 600 nm at 20 hpf to almost 5 µm at 25 hpf and thereafter (Suppl. Table 3). More bendable cilia, a more invariant position or possible breaking/rebuilding may account for a variable measurements at late stages (Suppl. Table 3). Overall 2 ciliated PNS pairs are present from 20 hpf onwards concomittant with actin rich microvilli extending towards the apical end.

Emerging CCs were analysed during development (Fig. 10, Suppl. Video 4) by correlating PNA binding, synaptotagmin gene expression and ciliary acetylated tubulin presence in PSNs (the latter both in green) in nuclear DAPI counterstained larvae of different stages. Strikingly, the earliest 18 hpf stages already showed a prominent PNA enrichment in the apex of the papillar rounding with a distal to proximal gradient of punctual PNA accumulations in more basal positions (Fig. 10A). This was paralleled by strong synaptotagmin > GFP expression in the cytoplasm and in nuclei of a great amount of papillar cells (Fig. 10B, C). During the following stages (Fig. 10D–L) the apical cap shaped PNA accumulation became more and more prominent with cells elongating and increasing the number of punctate PNA accumulations in the cytoplasm. Because the PNA dots were devoid of cytoplasmic GFP reporter they likely constitute the closed compartments of secretory vesicles of collocytes with more basally located nuclei (white arrows and stars, respectively, in Fig. 10C, F, I and L). Note that in the stage 24 hpf larval palp (Fig. 10J–L, Suppl. Video 5) both, a central, granule containing collocyte is visible next to a bulky PSN (both GFP positive) while the latter does not contain granules. CCs are thus the earliest, the most prominent and the most active cells in the developing papillae. This is consistent with the larger CC cell numbers counted in TEM cross sections.

Supplementary material related to this article can be found online at doi:10.1016/j.ydbio.2018.11.012.

A schematic overview of the time course of developmental events is summarized in Fig. 11 showing the appearance and expression levels of the various markers relative to the changing morphology. Overall, the Collocytes (CCs) arise and differentiate before the other cell types in the emerging palp primordium and produce secretory material deposited in the papillar apex, growing to an extended hyline cap. The CCs secretory activity is thus established before the morphogenetic changes of elongating palp cells and precedes the differentiation of PSNs and ACCs. More detailed analyses, with additional differentiation markers and by following dynamically the early division events, will determine in the future their exact ontogenetic relatedness and how the individual specification and differentiation occurs in the developing palp.

4. Discussion/conclusion

We propose discriminatory markers for the three cell types constituting exactly 20 cells in each of the three *Ciona* sensory adhesive organs. We newly introduce the collocyte (CC) marker PNA that visualizes the contents of secretory granules, the deposit of adhesive material in the hyaline cap and the adhesive plaques on the substrate. Strikingly, the production and deposition of the adhesive material starts very early and with the outgrowth of the papillae from the frontal head epithelium. This is accompanied with a rich accumulation of cytoskeletal actin filaments and microtubule bundles surrounding the elongating papillar apex and occurs prior to the differentiation marker expression of primary sensory neurons (PSNs) and axial columnar cells (ACCs), i.e. ciliary acetylated tubulin and βγ-crystallin, respectively.

Surprisingly, the 12 PNA positive collocytes turn out to be also strongly stained with the synaptotagmin reporter and may represent thus what was previously taken to be a 'second neuron' in the papillar extention (Imai and Meinertzhagen, 2007). Indeed, collocytes actually contain basal bodies (but no cilia) pointing to their birth from common precursors with the 4 PSNs, the latter being synaptotagmin and VgluT positive.

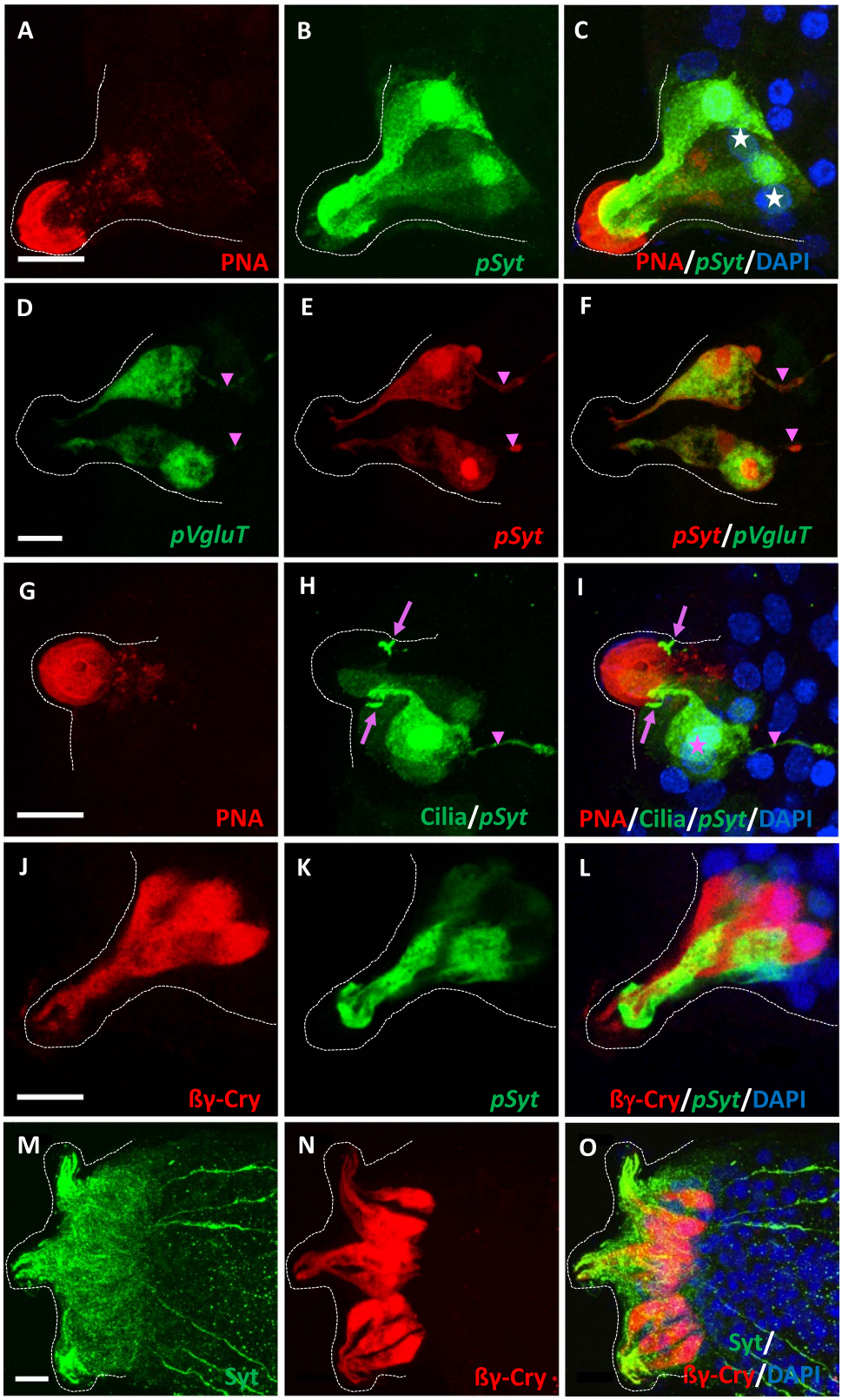

Fig. 7. Synaptotagmin is differentially expressed in the three papillar cell types. (A)–(L) Confocal projections of adhesive papillae in transgenic larvae (24 hpf) showing mosaic expression of the synaptotagmin reporters *pSyt* > GFP (A–C, G–L) or *pSyt* > mCherry (D–F): (A–C) *pSyt* > GFP signal (green) in PNA positive CCs (red) with basal nuclei (DAPI, blue). (D–F) *pSyt* > mCherry signal (red) in PSNs (*pVgluT* > GFP, green). (G-I) Synaptotagmin signal (*pSyt* > GFP, green) in PSNs with stained cilia (pink arrows, cilia in green from antibody labelling with acetylated tubulin), PSNs flank the PNA labeled CCs (red). Note the weak *pSyt* > GFP signal in CCs (weak green, central papilla in H, I). (J–L) Synaptotagmin reporter (*pSyt* > GFP, green) in double staining with ßγ-Crystallin antibody (ACCs, red) and DAPI (nuclei, blue). (M–O) Synaptotagmin antibody (green) in triple staining with ßγ-Crystallin antibody (ACC's, red), and DAPI (nuclei, blue). Note that the Synaptotagmin protein (M–O) seems present in all cell types (in contrast to the reporter). White stars on nuclei of CCs, pink arrows on cilia of PSNs, pink stars on nuclei of PSNs, and pink arrowheads on axons of PSNs. Scale bar: 10 µm.

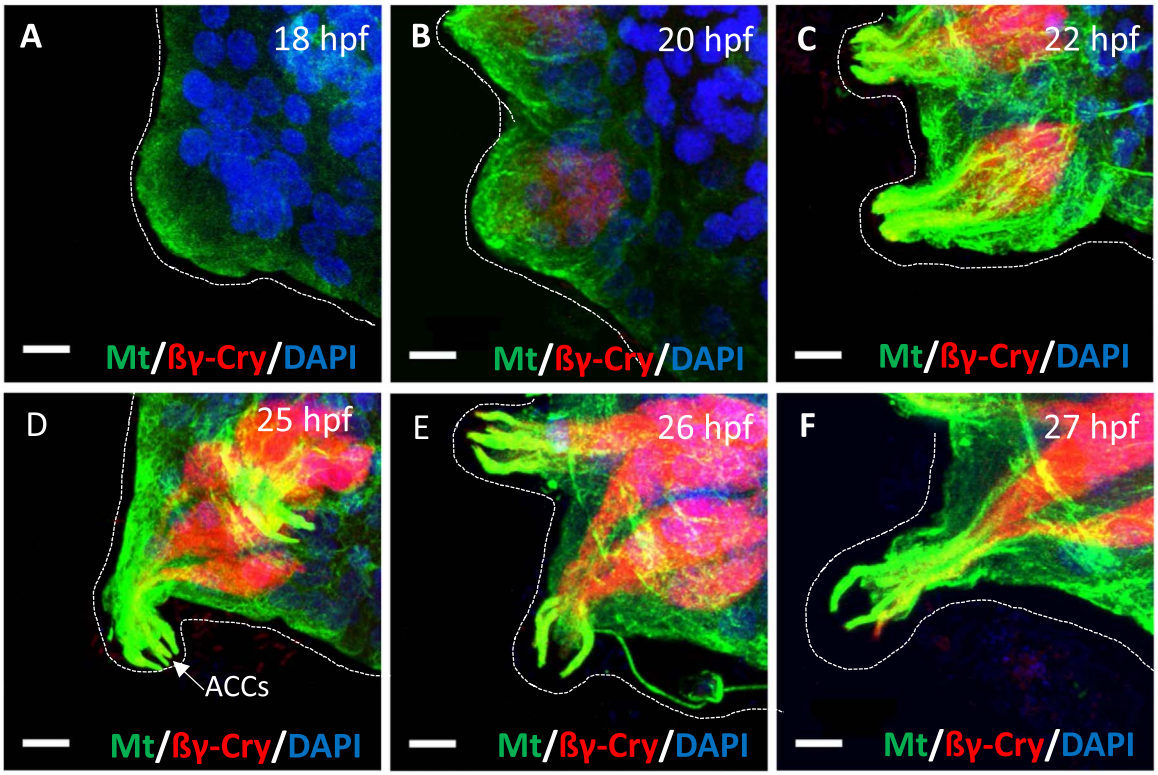

Fig. 8. Apical microtubule networks condensate before the differentiation of ACCs. (A)–(F) Confocal projections of adhesive papillae at different developmental time points (18–27 hpf) in triple labelling with α-Tubulin antibody (Mt, Microtubule green), ßγ-Crystallin antibody (in ACCs, red) and DAPI (nuclei, blue). Dotted lines outline the adhesive papillae. *ACCs* axial columnar cells. Scale bar: 10 μm.

The 4 ACCs correspond to the ßγ-crystallin positive cells extending their large protrusions far into the hyaline cap. From earlier studies we know that ßγ-crystallin is not secreted (Shimeld et al., 2005) and Islet is epistatically upstream of ßγ-crystallin to trigger both, its expression and the morphological changes of cellular elongation (Wagner et al., 2014). Due to the elongated shape of all cells we expect the collocyte and PSN markers to likewise depend on *islet* expression, although an independent regulation is possible, too.

The paired arrangement of cells within each papillar extension is intriguing and points to several invariant cleavage events of precursors in the papillar premordium arising at mid-gastrula stages from row six of the neural plate. The 4 ACCs and the 4 PSNs may have formed through either four asymmetric divisions (such as from surrounding collocyte precursors), or by one asymmetric and one symmetric division each, or by two consecutive symmetric divisions. The latter seems most likely for ACCs due to their equal size, regular, central position and their membrane links (Figs. 6 and S2, S3, S5 and S6). For the PSNs, a lateral, more segregated position suggests that each pair arose by one asymmetric division followed by a symmetric division to generate the twinned ciliated PSN pairs comparable to the last symmentric division in PSNs of the epidermal midline (Pasini et al., 2006). In contrast, the 12 CCs probably underwent several symmetric divisions but likely encompassed an asymmetric event that may have occurred either early (such as to form central ACC precursors) or later in two CC precursors (such as to form 2 laterally positioned PSN precursors). Nevertheless, a different timing of divisions could also generate a non-logarithmic cell number. Following the cell division from the 6-row stage onwards using lineage trackers should clarify their precise ontogeny. Indeed, the overall cell number we obtained in the papillae of adhesion competent larvae (60 plus 6–12 accessory cells present in the lower papillar body, blue in Figs. S2–S4) corresponds to previous cell counts obtained for the papillar region in midtailbud larvae, with 5 consecutive cell divisions predicted upon palp precursors labelling (Nishida, 1987) or counting 71 cells upon Phalloidin staining (Nakamura et al., 2012).

We found only one type of collocytes, and by their size and position they compare to the C2 type collocytes defined by Cloney (1977). Interestingly, however, we observe two types of granules, which we could distinguish well in TEM from cryofixed samples: the larger granule type was more ellipsoid in shape and likely contained glycoproteinaceous material while the slightly smaller, round granules had an undulated limiting membrane and contained a polysaccharide-rich fibrous material. Further studies are required to determine the exact contents and function of the two granule types. It is tempting to speculate that the contents of the two granules need to mix to form a crosslinking adhesive material for effective larval attachment.

Interestingly, we found that the synaptotagmin promoter is activated in collocytes, which also showed activation in the flanking neurons (PSNs) as previously described (Imai and Meinertzhagen, 2007). The early and strong *syt* reporter gene expression in both, collocytes and neurons but also the presence of basal bodies in the non-ciliated collocytes (Fig. 4B, F) may hint to their common precursor origin. Synaptotagmins (Syts) are a large protein family with their best known member (Syt1) well characterised as Ca^{2+} sensor for synchronised and rapid exocytosis (reviewed in Xie et al., 2017). Interestingly, Syts also play an important role in the coupling of endocytosis and exocytosis (reviewed in Liang et al., 2017; Xie et al., 2017). Interestingly, in sea urchin Syt1 plays a crucial role in oocyte cortical granule exocytosis where it is tethered to the granule membranes stably docked in a hemifused state and relieved by Ca^{2+} for rapid exocytosis (Wu et al., 2006).

While we have used the reporter gene for synaptotagmin 1, several evolutionary conserved synaptotagmins exist and it will be interesting to screen their presence and role in the secretory process of larval attachment. Both, *Ciona intestinalis* and *Ciona savignyi* have a rather compact and likely reduced repertoire of probably 9 Syt like molecules compared to many more in other marine invertebrates (Craxton, 2010), with 19 members in a cephalochordate or 28 in a cnidarian, while the vertebrate repertoire extends to 25 but is restricted to similar

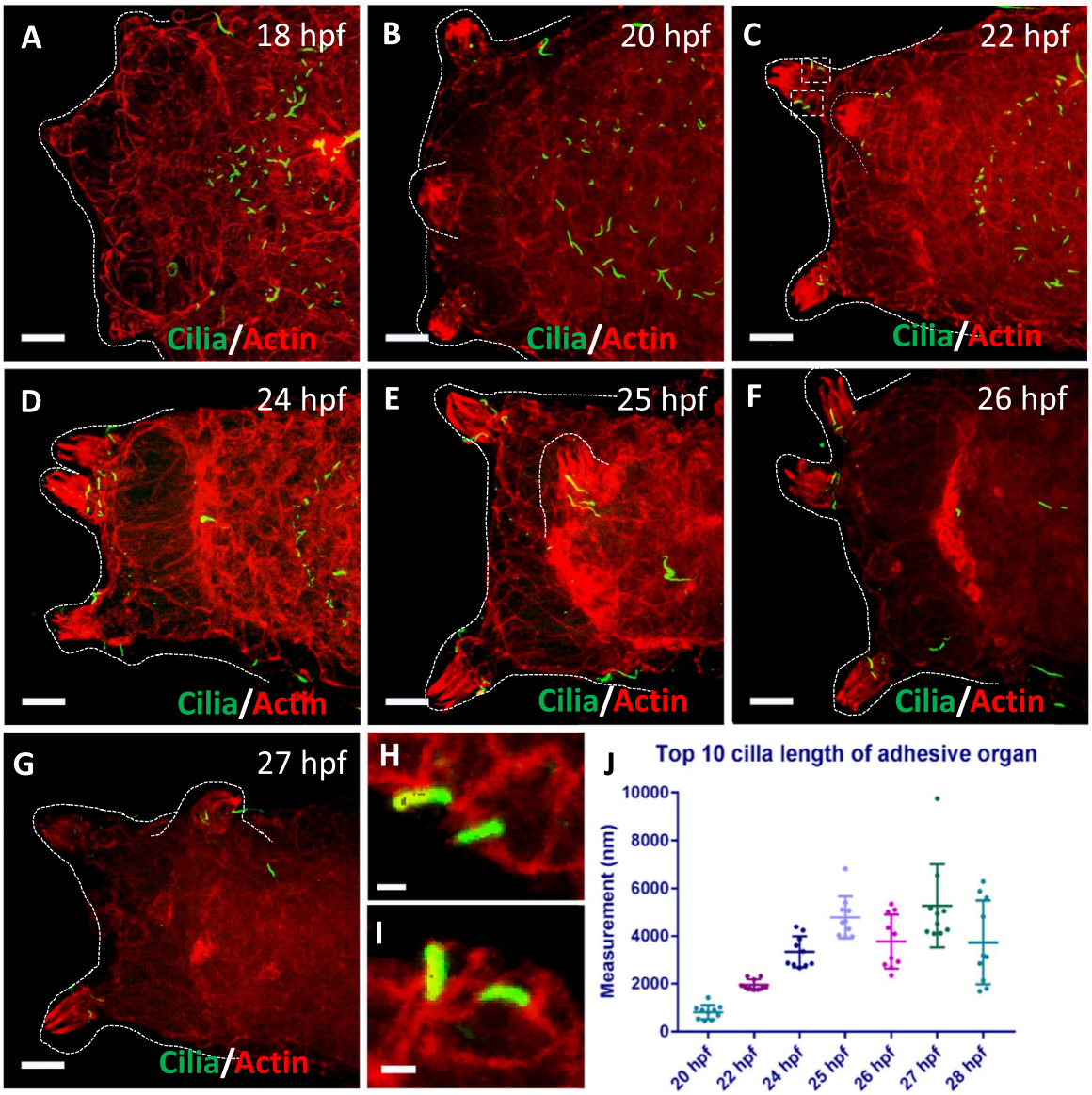

Fig. 9. PSNs lengthen their cilia while actin bundles elongate in apical protrusions. (A–G) Confocal projection of adhesive papillae at different developmental time points (18–27 hpf) in double labelling with phalloidin (Actin, red) and acetylated tubulin antibody (Cilia, green) (H, I) Zoom of rectangular areas in C. (J) Measurement of the cilia (ten longest) increasing of length during larval development. Dotted lines outline the adhesive papillae. Scale bar: (A–G) 10 µm, (H, I) 1 µm.

9–12 in ecdysozoans including fruit flies or nematodes. Interestingly, in most species analysed, Syt1 and Syt7 are present and have preserved the Ca^{2+} binding motifs (except for Syt7 in nematodes), while varying versions of Syts exist for less known non-Ca^{2+}-functions.

We also observe a dynamic change in the orientation and density of the cytocytoskeletal components actin and tubulin during the papillar development, with an early and strong apical enrichment in the organ that thins out with time in the proximal papillae but intensifies in the distal most, apical regions, notably the papillar protrusion of ACCs.

Consistently, the cytocytoskeletal architecture, of both actin and tubulin, is known to play an important role during regulated exocytosis, with notably actin tightly coordinating the delivery of secretory granules to the sites of fusion with the plasma membrane (reviewed in Porat-Shliom et al., 2013). Interestingly, both a rapid fusion of smaller vesicles and the slow accumulation of larger granules of more sustained and energetically less favorable responses are hereby controlled, with contractile actomyosin complexes likely providing the energy to enlarge the fusion pores and to expulse very large cargo into the extracellular space. These fundamental two roles of actin may explain the observed early papillar longitudinal and later strongly apically focused arrays of the cytoskeleton. The close proximity of collocytes to ACCs, but also PSNs allows for speculations on a collaborative role among cell types in vesicular tethering. It will be interesting to specifically perturb both, the individual cytoskeletal components as well as to consider the controlled and cell type specific molecular interference in the context of larval adhesion.

Because the secretion during larval attachment may include cellulose material for the spreading of the ascidian tunic in immediately succeeding steps of metamorphosis, it worth considering that the cellulase secretion is similar to that of other proteins (reviewed in Yan and Wu, 2013) with very recent data on bacterial cellulose fibre secretion emerging (Krasteva et al., 2017).

Intriguing evolutionary conclusions may be drawn from our study concerning the emergence of the cranial placode derived sense organs in the vertebrate ‘new head’. Our cellular analyses favor the hypothesis that the triangularly arranged papillae/palps of the tunicates resemble simple head sensory organs that evolved from an anterior proto-placodal region present in the vertebrate-tunicate ancestor and that

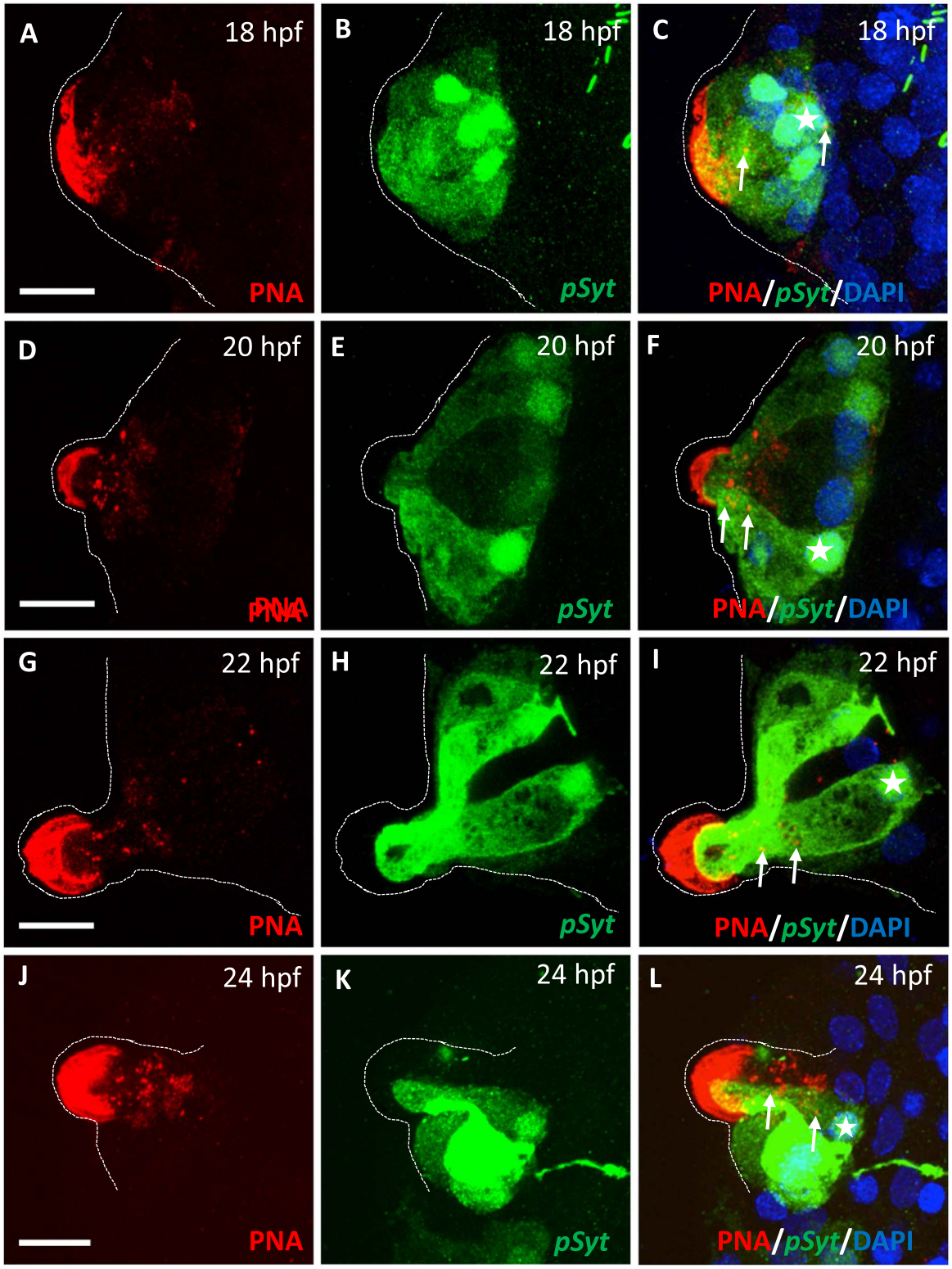

Fig. 10. Collocyte features are distinguished earliest during palp development. (A–L) Confocal projection of single adhesive papilla at different developmental time points (18–24 hpf) in synaptotagmin reporter transgenic larvae (*pSyt* > GFP, CCs and/or PSNs, green) labeled with PNA (CCs and hyaline cap, red) and DAPI (nuclei, blue). Note that both, the granular PNA staining (white arrows) and the cytoplasmic and nuclear (white stars) *pSyt* > GFP signal are labelling the collocytes, Scale bars: 10 µm.

unites features of the olfactory and visual cellular programs found in vertebrates. Known as key vertebrate innovations, the cranial placodes are defined as transitory embryonic regions arising from the anterior neural plate border to form sensory epithelia of massively proliferating precursors of neural and non-neural cell types for paired, high density arrays of specialized sensory and accessory cells of the vertebrate head sensory organs (reviewed in Schlosser et al., 2014). Two major preplacodal fields in vertebrates give rise to three separate regions each: the anterior olfactory, lens and adenohypophyseal placodes and the more posterior otic, lateral line and epibranchial placodes. These common embryonic fields likely co-existed in the vertebrate-tunicate ancestor and in tunicates were so far largely attributed to the oral and

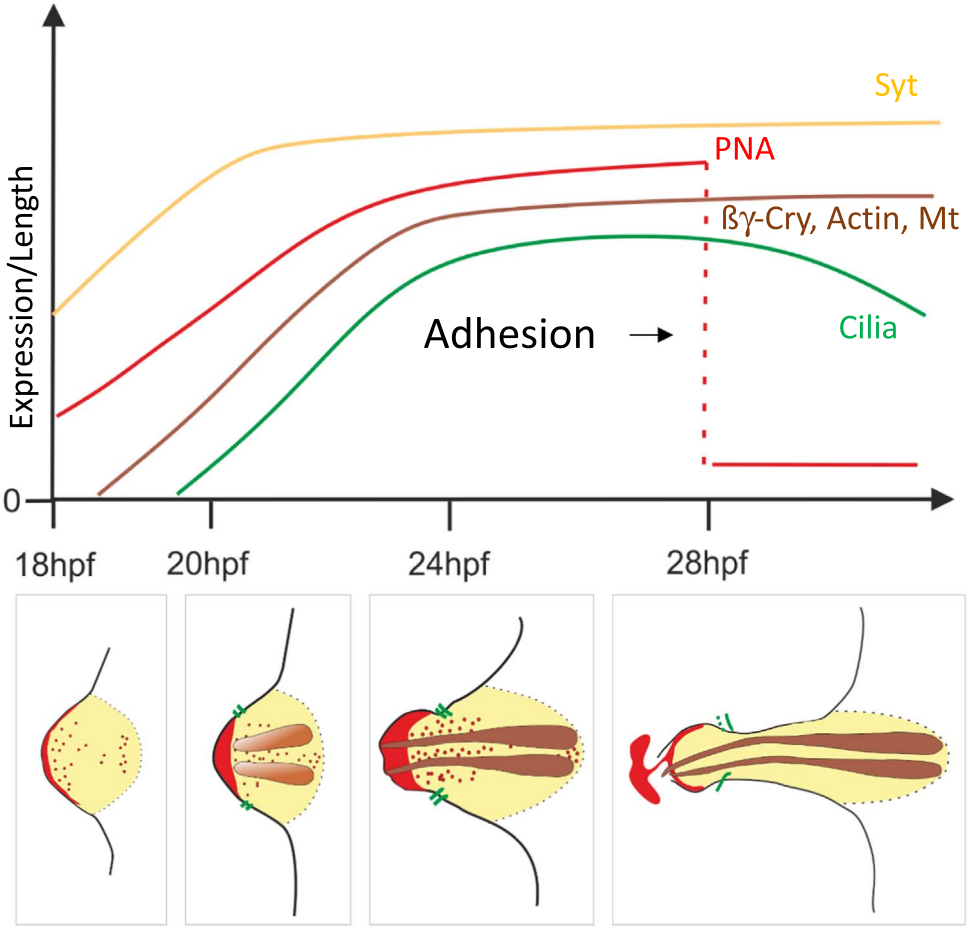

Fig. 11. Developmental dynamics of papillar markers and morphological changes. Developmental changes in larval papillae of *Ciona* depicted between 18 hpf and 28 hpf: expression changes of cell type specific differentiation markers (graph) are associated with morphological changes (bottom schemes) at the indicated developmental stages (horizontal time line).Differentiation markers for collocytes, (Synaptotagmin reporter gene activity, Syt, yellow, and PNA in secretory granules, red) are present in earliest papillar bud stages (18 hpf), increase and reach a maximum at 24 hpf. ACC and PSN differentiation markers (ßγ-Crystallin and Cilia) appear thereafter (between 18 hpf and 20 hpf) along with cytoskeletal actin and microtubules (Mt) that accumulate in the elongating apical ACC extensions, likely guiding both, the elongation process of papillae and, the granular transport towards the hyaline cap, but stagnate at the later stages. Cilia lengthen steadily but appear shortened again at adhesion competent stages (28 hpf), possibly upon papillar touching, often having released some PNA labeled glue material from their apical hyline cap. Color code: yellow for syt, red for PNA in adhesive granules, hyaline cap and glue, green lines for cilia, brown for ßγ-Crystallin in ACCs (but also for Actin and Mt), black line for the tunic.

atrial siphon primordia (Mazet and Shimeld, 2005; Graham and Shimeld, 2013). A homology of tunicate papillae to the rostral-most olfactory placode was previously found unlikely due to a ventral position relative to the 'mouth' (the far dorsally positioned oral siphon primordium) (Manni et al., 2004). Several lines of evidence, however, lead us to propose that the anterior-most protoplacodal territory in tunicates has evolved a simple head sensory organ, the larval papillae, that indeed shares homologies to the olfactory and visual placode derivatives in vertebrates.

Firstly the papillae arise from a single anterior-most neural border territory that is patterned similarly to that in vertebrates (Saint-Jeannet and Moody, 2014). A single anterior bilateral pair of ancestor blastomeres (a6.5), most convincingly traceable by the invariant cellular lineage in tunicates, carries the pre-neural state (FGF induced, expressing Otx, then DMRT) and asymmetrically divides into neural precursors (adjacent to the FGF source, expressing ZicL and forming the larval brain) and neural border cells (low FGF, FoxC expression, forming the papillae and the neurohypophysal/aATEN precursors) (reviewed in Pennati and Rothbacher, 2015). A common source of localized precursors at the neural border thus diversifies into the 3 specialized cell types of the *Ciona* sensory adhesive organ. Secondly, the molecular repertoirs that pattern and compartmentalize the pre-placodal ectoderm are greatly conserved and likely preceded the advent of vertebrates. A shared set of target genes common to tunicates and vertebrates include the above mentioned upstream regulators FGF, Otx, Dmrt, FoxC and a number of sensory cell type markers (Schlosser et al., 2014; Horie et al., 2018). Thirdly, a subfunctionalization from ancestral cell types is thought to have allowed for the complexity in the vertebrate head sensory organs (Patthey et al., 2014). The aATENs of tunicates were compared to such ancestral ciliated secretory neurons uniting properties found in different cell types of the vertebrate olfactory organ (Abitua et al., 2015). Furthermore, here we show in great detail that the tunicate papillar primordium already shows a subfunctionalization into mechanosensory, secretory and chemosensory function alltogether forming an intact head sensory organ. Hereby, two sub-groups of precursors likely emerged with a closer developmental history being shared between the ciliated primary sensory neurons (PSNs) and the secretory collocytes (CCs) both featuring paired basal bodies and an early activation of pSyt as opposed to the Axial columnar cells (ACCs) that express ßγ-crystallin of the lens fibre protein family. Interestingly, lens marker expression was proposed as ground state for all sensory placodes in vertebrates (Bailey et al., 2006) and it is therefore likely that such character preexisted in the ancestral chordate. Notably, much of the gene regularly circuitry of ßγ-crystallin seems conserved as the *Ciona* regulatory region also drives expression in both, the ascidians brain derived light sensory organ and the vertebrate lens (Shimeld et al., 2005; Graham and Shimeld, 2013). Indeed, additional effectors of the vertebrate photo-sensing machinery

such as arrestin and Rx, present in the larval brain visual cells, show additional expression domains in the papillae (Oonuma et al., 2016; D'Aniello et al., 2006) whereby Ci-arrestin resembles both, visual and non-visual arrestins found in vertebrates (Nakagawa et al., 2002). Recently, a number of common molecular components are being discovered in different sensory cell types of invertebrates across metazoans despite a lack of proper head sensory organs (Schlosser, 2018). Finally, the vertebrate sensory organs greatly depend on extensive precursor expansion. In tunicates, proliferation is generally kept to a minimum and many larval structures are not maintained into adulthood as in vertebrates, including the papillae. Nevertheless, the 20 papillar cells with 16 secretory cells in each papillar organ of *Ciona,* constitute an ordered array in a pseudo-stratified epithelium that reaches much greater numbers and complexity in other ascidian species (reviewed in Pennati and Rothbacher, 2015). Indeed, more elaborated invaginations and expanded arrays of additional cell types are found in the more complex, everting papillae counting up to 10^3 cells in some ascidian species (Cloney, 1977). Overall, the tunicate larval sensory adhesive organ may resemble an evolutionary snapshot of an ancestral chordate program featuring common cellular, molecular and regulative components of secretion, olfaction and photo-sensation combined in a simple rostral organ. An ancestral rostral olfactory-lens placodal field that produced the sensory adhesive organs in tunicates likely evolved stepwise into separate and highly expanded, sophisticated epithelia for smell and vision in vertebrates.

Overall the accessability of the ascidian development with the presented fundamental knowledge on the papillar cell types, their number, cellular and subcellular architecture, combined with our data on individual or common molecular repertoires will be instrumental in answering many open questions on the mechanisms controlling papillar adhesion. This knowledge will be important not only for understanding adhesion in wet conditions but analysing this crucial larval stage to trigger metamorphosis and apoptosis, is generally relevant for our fundamental understanding of mechanosensory and secretory function in development, evolution and human disease.

Acknowledgements

We acknowledge excellent technical assistance in HPF of Barbara Witting and Karin Gutleben, Division of Histology and Embryology, Innsbruck Medical University. We are grateful to Theodora Vasakou and Kevin Grüner for help in TEM false coloring and image acquisition and Bert Hobmayer for comments on the manuscript. Research reported in this publication was supported by the Austrian Academy of Sciences ÖAW DOC 24699 (FZ), the Austrian Science Fund FWF 25404 (PL), the University Innsbruck Vicerectorate for Research Sonderförderung 214947 (UR), the Nachwuchsförderung Universität Innsbruck (FZ and JW) and the Autonome Provinz Bozen (JW).

Appendix A. Supplementary material

Supplementary data associated with this article can be found in the online version at doi:10.1016/j.ydbio.2018.11.012.

References

Abitua, P.B., Wagner, E., Navarrete, I.A., Levine, M., 2012. Identification of a rudimentary neural crest in a non-vertebrate chordate. Nature 492, 104–107.
Abitua, P.B., Gainous, T.B., Kaczmarczyk, A.N., Winchell, C.J., Hudson, C., Kamata, K., Nakagawa, M., Tsuda, M., Kusakabe, T.G., Levine, M., 2015. The pre-vertebrate origins of neurogenic placodes. Nature 524, 462–465.
Aldred, N., Clare, A.S., 2014. Mini-review: impact and dynamics of surface fouling by solitary and compound ascidians. Biofouling 30, 259–270.
Bailey, A.P., Bhattacharyya, S., Bronner-Fraser, M., Streit, A., 2006. Lens specification is the ground state of all sensory placodes, from which FGF promotes olfactory identity. Dev. Cell 11, 505–517.
Caicci, F., Zaniolo, G., Burighel, P., Degasperi, V., Gasparini, F., Manni, L., 2010. Differentiation of papillae and rostral sensory neurons in the larva of the ascidian *Botryllus schlosseri* (Tunicata). J. Comp. Neurol. 518, 547–566.
Cloney, R.A., 1977. Larval adhesive organs and metamorphasis in ascidians I fine structure of everting papillae of *Distaplia occidentalis*. Cell Tiss. Res 183, 423–444.
Craxton, M., 2010. A manual collection of *Syt*, *Esyt*, *Rph3a*, *Rph3al*, *Doc2*, and *Dblc2* genes from 46 metazoan genomes – an open access resource for neuroscience and evolutionary biology. BMC Genom. 11, 37.
D'Aniello, S., D'Aniello, E., Locascio, A., Memoli, A., Corrado, M., Russo, M.T., Aniello, F., Fucci, L., Brown, E.R., Branno, M., 2006. The ascidian homolog of the vertebrate homeobox gene Rx is essential for ocellus development and function. Differentiation 74, 222–234.
Davidson, B., Swalla, B.J., 2002. A molecular analysis of ascidian metamorphosis reveals activation of an innate immune response. Development 129, 4739–4751.
Dehal, P., Satou, Y., Campbell, R.K., Chapman, J., Degnan, B., De Tomaso, A., Davidson, B., Di Gregorio, A., Gelpke, M., Goodstein, D.M., Harafuji, N., Hastings, K.E., Ho, I., Hotta, K., Huang, W., Kawashima, T., Lemaire, P., Martinez, D., Meinertzhagen, I.A., Necula, S., Nonaka, M., Putnam, N., Rash, S., Saiga, H., Satake, M., Terry, A., Yamada, L., Wang, H.G., Awazu, S., Azumi, K., Boore, J., Branno, M., Chin-Bow, S., DeSantis, R., Doyle, S., Francino, P., Keys, D.N., Haga, S., Hayashi, H., Hino, K., Imai, K.S., Inaba, K., Kano, S., Kobayashi, K., Kobayashi, M., Lee, B.I., Makabe, K.W., Manohar, C., Matassi, G., Medina, M., Mochizuki, Y., Mount, S., Morishita, T., Miura, S., Nakayama, A., Nishizaka, S., Nomoto, H., Ohta, F., Oishi, K., Rigoutsos, I., Sano, M., Sasaki, A., Sasakura, Y., Shoguchi, E., Shin-i, T., Spagnuolo, A., Stainier, D., Suzuki, M.M., Tassy, O., Takatori, N., Tokuoka, M., Yagi, K., Yoshizaki, F., Wada, S., Zhang, C., Hyatt, P.D., Larimer, F., Detter, C., Doggett, N., Glavina, T., Hawkins, T., Richardson, P., Lucas, S., Kohara, Y., Levine, M., Satoh, N., Rokhsar, D.S., 2002. The draft genome of *Ciona intestinalis*: insights into chordate and vertebrate origins. Science 298, 2157–2167.
Delsuc, F., Brinkmann, H., Chourrout, D., Philippe, H., 2006. Tunicates and not cephalochordates are the closest living relatives of vertebrates. Nature 439, 965–968.
Dolcemascolo, G., Pennati, R., De Bernardi, F., Damiani, F., Gianguzza, M., 2009. Ultrastructural comparative analysis on the adhesive papillae of the swimming larvae of three ascidian species. Invert. Surv. J. 6, S77–S86.
Eisenman, E.A., Alfert, M., 1982. A new fixation procedure for preserving the ultrastructure of marine invertebrate tissues. J. Microsc. 125, 117–120.
Feoktistova, M., Geserick, P., Leverkus, M., 2016. Crystal violet assay for determining viability of cultured cells. Cold Spring Harb. Protoc., (2016, pdb prot087379).
Gammoudi, M., Salvenmoser, W., Tekaya, S., Egger, B., 2016. Ultrastructure of the ovary and oogenesis in the flatworm *Prosthiostomum siphunculus* (Polycladida, Cotylea). Cell Biol. Int. 40 (11), 1174–1186.
Gilchrist, M.J., Sobral, D., Khoueiry, P., Daian, F., Laporte, B., Patrushev, I., Matsumoto, J., Dewar, K., Hastings, K.E.M., Satou, Y., Lemaire, P., Rothbächer, U., 2015. A pipeline for the systematic identification of non-redundant full-ORF cDNAs for polymorphic and evolutionary divergent genomes: Application to the ascidian Ciona intestinalis. Dev. Bio. 404, 149–163.
Graham, A., Shimeld, S.M., 2013. The origin and evolution of the ectodermal placodes. J. Anat. 222, 32–40.
Hennebert, E., Wattiez, R., Flammang, P., 2011. Characterisation of the carbohydrate fraction of the temporary adhesive secreted by the tube feet of the sea star *Asterias rubens*. Mar. Biotechnol. 13, 484–495.
Hess, M.W., Hesse, M., 1994. Ultrastructural observations on anther tapetum development of freeze-fixed *Ledebouria socialis* Roth (Hyacinthaceae). Planta 192, 421–430.
Horie, T., Kusakabe, T., Tsuda, M., 2008. Glutamatergic networks in the *Ciona intestinalis* larva. J. Comp. Neurol. 508, 249–263.
Horie, R., Hazbun, A., Chen, K., Cao, C., Levine, M., Horie, T., 2018. Shared evolutionary origin of vertebrate neural crest and cranial placodes. Nature 560, 228–232.
Imai, K.S., Levine, M., Satoh, N., Satou, Y., 2006. Regulatory blueprint for a chordate embryo. Science 312.
Imai, J.H., Meinertzhagen, I.A., 2007. Neurons of the ascidian larval nervous system in *Ciona intestinalis*: II. Peripheral nervous system. J. Comp. Neurol. 501, 335–352.
Karaiskou, A., Swalla, B.J., Sasakura, Y., Chambon, J.P., 2015. Metamorphosis in solitary ascidians. Genesis 53, 34–47.
Kari, W., Zeng, F., Zitzelsberger, L., Will, J.P., Rothbächer, U., 2016. Embryo microinjection and electroporation in the chordate *Ciona intestinalis*. J. Vis. Exp..
Katsuyama, Y., Matsumoto, J., Okada, T., Ohtsuka, Y., Chen, L., Okado, H., Okamura, Y., 2002. Regulation of synaptotagmin gene expression during ascidian embryogenesis. Dev. Biol. 244, 293–304.
Kimura, Y., Yoshida, M., Morisawa, M., 2003. Interaction between noradrenaline or adrenaline and the β1-adrenergic receptor in the nervous system triggers early metamorphosis of larvae in the ascidian, *Ciona savignyi*. Dev. Biol. 258, 129–140.
Krasteva, P.V., Bernal-Bayard, J., Travier, L., Martin, F.A., Kaminski, P.A., Karimova, G., Fronzes, R., Ghigo, J.M., 2017. Insights into the structure and assembly of a bacterial cellulose secretion system. Nat. Commun. 8, 2065.
Lane, D.J.W., 1973. Attachment of the larva of the ascidian *Diplosoma listerianum*. Mar. Biol. 21, 47–58.
Lengerer, B., Hennebert, E., Flammang, P., Salvenmoser, W., Ladurner, P., 2016. Adhesive organ regeneration in *Macrostomum lignano*. BMC Dev. Biol. 16, 20.
Lengerer, B., Pjeta, R., Wunderer, J., Rodrigues, M., Arbore, R., Schärer, L., Berezikov, E., Hess, M.W., Pfaller, K., Egger, B., Obwegeser, S., Salvenmoser, W., Ladurner, P., 2014. Biological adhesion of the flatworm *Macrostomum lignano* relies on a duo-gland system and is mediated by a cell type-specific intermediate filament protein. Front. Zool. 11, 12.
Liang, K., Wei, L., Chen, L., 2017. Exocytosis, endocytosis, and their coupling in excitable cells. Front. Mol. Neurosci. 10, 109.
Manni, L., Lane, N.J., Joly, J.S., Gasparini, F., Tiozzo, S., Caicci, F., Zaniolo, G., Burighel, P., 2004. Neurogenic and non-neurogenic placodes in ascidians. J. Exp. Zool. Part B

Mol. Dev. Evol. 302, 483–504.
Mazet, F., Shimeld, S.M., 2005. Molecular evidence from ascidians for the evolutionary origin of vertebrate cranial sensory placodes. J. Exp. Zool. Part B Mol. Dev. Evol. 304, 340–346.
Nakamura, M.J., Terai, J., Okubo, R., Hotta, K., Oka, K., 2012. Three-dimensional anatomy of the *Ciona intestinalis* tailbud embryo at single-cell resolution. Dev. Biol. 372, 274–284.
Nakagawa, M., Orii, H., Yoshida, N., Jojima, E., Horie, T., Yoshida, R., Haga, T., Tsuda, M., 2002. Ascidian arrestin (Ci-arr), the origin of the visual and nonvisual arrestins of vertebrate. Eur. J. Biochem. 269, 5112–5118.
Nakayama-Ishimura, A., Chambon, J.P., Horie, T., Satoh, N., Sasakura, Y., 2009. Delineating metamorphic pathways in the ascidian *Ciona intestinalis*. Dev. Biol. 326 (2), 357–367.
Nishida, H., 1987. Cell lineage analysis in ascidian embryos by intracellular injection of a tracer enzyme. III. Up to the tissue restricted stage. Dev. Biol. 121, 526–541.
Oonuma, K., Tanaka, M., Nishitsuji, K., Kato, Y., Shimai, K., Kusakabe, T.G., 2016. Revised lineage of larval photoreceptor cells in Ciona reveals archetypal collaboration between neural tube and neural crest in sensory organ formation. Dev. Biol. 420, 178–185.
Pasini, A., Amiel, A., Rothbächer, U., Roure, A., Lemaire, P., Darras, S., 2006. Formation of the ascidian epidermal sensory neurons: insights into the origin of the chordate peripheral nervous system. PLoS Biol. 4, e225.
Patthey, C., Schlosser, G., Shimeld, S.M., 2014. The evolutionary history of vertebrate cranial placodes-I: cell type evolution. Dev. Biol. 389 (1), 82–97.
Pennati, R., Zega, G., Groppelli, S., De Bernardi, F., 2007. Immunohistochemical analysis of adhesive papillae of *Botryloides leachi* (Chordata, Tunicata). Ital. J. Zool. 74, 325–329.
Pennati, R., Rothbacher, U., 2015. Bioadhesion in ascidians: a developmental and functional genomics perspective. Interface Focus 5, 20140061.
Porat-Shliom, N., Milberg, O., Masedunskas, A., Weigert, R., 2013. Multiple roles for the actin cytoskeleton during regulated exocytosis. Cell Mol. Life Sci. 70, 2099–2121.
Rodrigues, M., Ostermann, T., Kremeser, L., Lindner, H., Beisel, C., Berezikov, E., Hobmayer, B., Ladurner, P., 2016. Profiling of adhesive-related genes in the freshwater cnidarian *Hydra magnipapillata* by transcriptomics and proteomics. Biofouling 32 (9), 1115–1129.
Roure, A., Rothbächer, U., Robin, F., Kalmar, E., Ferone, G., Lamy, C., Missero, C., Mueller, F., Lemaire, P., 2007. A multicassette Gateway vector set for high throughput and comparative analyses in *Ciona* and vertebrate embryos. PLoS One 2, e916.
Saint-Jeannet, J.P., Moody, S.A., 2014. Establishing the pre-placodal region and breaking it into placodes with distinct identities. Dev. Biol. 389, 13–27.
Sakurai, D., Goda, M., Kohmura, Y., Horie, T., Iwamoto, H., Ohtsuki, H., Tsuda, M., 2004. The role of pigment cells in the brain of ascidian larva. J. Comp. Neurol. 475, 70–82.
Salvenmoser, W., Egger, B., Achatz, J.G., Ladurner, P., Hess, M.W., 2010. Electron microscopy of flatworms. Electron Microsc. Model Syst., 307–330.
Sasakura, Y., Mita, K., Ogura, Y., Horie, T., 2012. Ascidians as excellent chordate models for studying the development of the nervous system during embryogenesis and metamorphosis. Dev. Growth Differ. 54 (3), 420–437.
Schlosser, G., Patthey, C., Shimeld, S.M., 2014. The evolutionary history of vertebrate cranial placodes II. Evolution of ectodermal patterning. Dev. Biol. 389 (1), 98–119.
Schlosser, G., 2018. A short history of nearly every sense – the evolutionary history of vertebrate sensory cell types. Integr. Comp. Biol. 58, 301–316.
Shimeld, S.M., Purkiss, A.G., Dirks, R.P., Bateman, O.A., Slingsby, C., Lubsen, N.H., 2005. Urochordate betagamma-crystallin and the evolutionary origin of the vertebrate eye lens. Curr. Biol.: CB 15, 1684–1689.
Stolfi, A., Gandhi, S., Salek, F., Christiaen, L., 2014. Tissue-specific genome editing in *Ciona* embryos by CRISPR/Cas9. Development 141, 4115–4120.
Takamura, K., Minamida, N., Okabe, S., 2010. Neural map of the larval central nervous system in the Ascidian *Ciona intestinalis*. Zool. Sci. 27, 191–203.
Tassy, O., Dauga, D., Daian, F., Sobral, D., Robin, F., Khoueiry, P., Salgado, D., Fox, V., Caillol, D., Schiappa, R., Laporte, B., Rios, A., Luxardi, G., Kusakabe, T., Joly, J.S., Darras, S., Christiaen, L., Contensin, M., Auger, H., Lamy, C., Hudson, C., Rothbächer, U., Gilchrist, M.J., Makabe, K.W., Hotta, K., Fujiwara, S., Satoh, N., Satou, Y., Lemaire, P., 2010. The ANISEED database: digital representation, formalization, and elucidation of a chordate developmental program. Genome Res. 20, 1459–1468.
Thiéry, J.P., 1967. Mise en évidence des polysaccharides sur coupes fines en microscopie électronique. J. Microsc. 6, 987–1018.
Wagner, E., Stolfi, A., Choi, Y.G., Levine, M., 2014. Islet is a key determinant of ascidian palp morphogenesis. Development.
Wu, M.M., Buchanan, J., Luik, R.M., Lewis, R.S., 2006. Ca^{2+} store depletion causes STIM1 to accumulate in ER regions closely associated with the plasma membrane. J. Cell Biol. 174, 803–813.
Yan, S., Wu, G., 2013. Secretory pathway of cellulase: a mini-review. J. Cell Biol. 174 (6), 803–813.
Xie, Z., Long, J., Liu, J., Chai, Z., Kang, X., Wang, C., 2017. Molecular mechanisms for the coupling of endocytosis to exocytosis in neurons. Front. Mol. Neurosci. 10, 47.